Optimization of Threshold Current Density for $Al_{0.01}Ga_{0.99}N$/GaN Multiple Quantum Well Laser

A thesis

Submitted to the Council of the College of Education for Pure Science Ibn Al-Haitham, University of Baghdad in partial fulfillment of requirements for the degree of Master of Science in Physics

By

Kzal Mohammed Qader

B.Sc. Physics (University of Baghdad) 2014

Supervised by

Dr. Ebtisam M-T. Salman

2017 A.C   **1438 A.**

بسم الله الرحمن الرحيم

﴿ إِنَّا أَنْزَلْنَاهُ فِي لَيْلَةِ الْقَدْرِ ۝ وَمَا أَدْرَاكَ مَا لَيْلَةُ الْقَدْرِ ۝ لَيْلَةُ الْقَدْرِ خَيْرٌ مِنْ أَلْفِ شَهْرٍ ۝ تَنَزَّلُ الْمَلَائِكَةُ وَالرُّوحُ فِيهَا بِإِذْنِ رَبِّهِمْ مِنْ كُلِّ أَمْرٍ ۝ سَلَامٌ هِيَ حَتَّى مَطْلَعِ الْفَجْرِ ۝ ﴾

صدق الله العلي العظيم

سورة القدر

Dedication

To

The martyrs of Iraq

Father & mother

Brother and sisters

My supervisor

Supervisor's Certification

I certify that this thesis entitled **"Optimization of Threshold Current Density for $Al_{0.01}Ga_{0.99}N$/GaN Multiple Quantum Well Laser"** was prepared by (**Kzal Mohammed Qader**), under my supervision at Department of Physics, Collage of Education for Pure Science/ Ibn Al-Haitham, University of Baghdad as partial fulfillment of the requirement for the degree of Master of Science in Physics.

Signature:

Name: Dr. Ebtisam M-T. Salman

Date: 15 / 10/ 2017

Title: Instructor

In view of available recommendation, I forward this thesis for debate by the examining committee

Signature:

Name: Dr. Kareem Ali Jasim

Date: 18/ 10 / 2017

Title: Professor

Address: Head of Department of Physics

Collage of Education for Pure Science/ Ibn Al-Haitham

University of Baghdad

Examining Committee Certification

We certify that we have read this thesis entitled: **"Optimization of Threshold Current Density for $Al_{0.01}Ga_{0.99}N/GaN$ Multiple Quantum Well Laser"** an examining committee, examined the student" **Kzal Mohammed Qader**" in its content and what standing as a thesis for the degree of Master of Science in Physics

Signature:

Name: Dr. Ahmed Farhan Atwan

Title: Professor

Date: 13-12-2017

(Chairman)

Signature:

Name: Dr. Mohammed Salman Mohammed

Title: Assistant Professor

Date: 14/12/2017

(Member)

Signature:

Name: Dr. Abdul Kareem Abdul Hussein Kareem

Title: Instructor
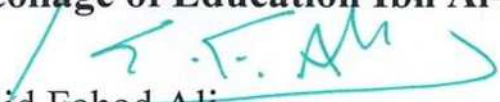
Date: 18/12/2017

(Member)

Signature:

Name: Dr. Ebtisam M-T. Salman

Title: Instructor

Date: 12/12/2017

(Member,Supervisor)

Approved for collage of Education Ibn Al-Haitham

Signature:

Name: Dr. Khalid Fahad Ali

Title: Professor

Date: 15/1/2018

Acknowledgments

At first, I thank Allah for helping me to complete this thesis.

I would like to express my deep appreciation to my supervisor Dr.Ebtisam M-T. salman for suggesting the topic of this thesis and for their unceasing guidance throughout the course of this work with kind, wisdom and experience.

Also, I extend my thanks and gratitude to the College of Education, Ibn al-Haytham for pure sciences and the chief of the Department of physics for their help and to all my professors.

I thank my friends who encouraged and help me during my research, I give my special thanks to my family for their constant support and encouragement.

Abstract

In this work, the theoretical study of the optimization of threshold current density for $Al_{0.01}Ga_{0.99}N$/GaN multiple quantum well laser structure is presented. This study is achieved through determination the best value of the affecting parameters on the threshold current and threshold current density of this structure such as wells number, barrier width, from emphases on the best value of optical confinement factor. Then calculated well width, reflectivity of cavity mirrors, cavity length, cavity width, average thickness of active region, mirror losses and threshold gain.

It is found that the best value of the optical confinement factor of $Al_{0.01}Ga_{0.99}N$/GaN multiple quantum well laser, when the number of wells (N_w=2) and barrier width (b=2 nm), when wavelength (λ=352 nm) in long ultraviolet (UVA) (320-400 nm) radiation range.

The optimum value for each of the threshold current density ($J_{th} = 3743$ A/cm^2) and threshold current ($I_{th} = 14.97$ mA) are obtained when the well width is (w= 4.3 nm), reflectivity of cavity mirrors (R$_1$=0. 75, R$_2$=0.9), cavity length (L=2mm), cavity width (W=200 nm), average thickness of active region (d= 10.6 nm), mirror losses (α$_m$=0.98 cm^{-1}) and threshold gain (g_{th}= 791 cm^{-1}) at this optimum values and temperature (T=300K).

Chapter One

Literature Review

Chapter Two

Theoretical Investigation

Chapter Three

Results and Discussion

LIST OF FIGURES

VII

LIST OF Tables

List Of Abbreviation	
SLs	Semiconductor lasers
LD	Laser Diode
LDs	Laser Diodes
CB	Conduction Band
CV	Valence Band
LED	Light emitting diode
DH	Double heterojunction
SH	Single heterojunction
CD	Compact Disk
HEMTs	High Electron Mobility Transistors
0 D	Zero Dimension
1D	One Dimension
2D	Two Dimension
QW	Quantum Well
QWR	Quantum Wire
QD	Quantum Dot
DOS	Density of States
SQW	Single quantum well
MQW	Multiple quantum well
TE	Transverse electric
TM	Transvers magnetic
CHCC	Conduction-hole conduction-conduction
CHSH	Conduction-heavy-hole-spin-split off
CHLH	Conduction-hole-light-heavy-hole

List of Symbols

Symbols	Description	Unite
h	Planck's constant	J.sec
$\hbar$	Plank's constant divided by 2π	J.sec
e	Electron charge	C
V_B	Potential barrier	V
V	Voltage	V
V	Potential energy	V
N	Carrier concentration	cm^{-3}
w	Well width	nm
d	average thickness of active region	nm
R	Reflectivity	none
n_r	Refractive index	non
n_{air}	Refractive index of the air	non
$E_{nx,ny,nz}$	The quantized energy levels	eV
n_x, n_y, n_z	Number of states	non
L	Cavity length	mm
W	Cavity width	nm
E_g	Energy gap	eV
E_g^{QW}	Energy band gap in the QW	eV
N, P	Electron and hole concentrations	cm^{-3}
m_o	Free electron mass	kg
m_e^*	Electron effective mass	kg
m_h^*	Hole effective mass	kg
m_{hh}	Heavy hole mass	kg
$|M_{ave}|^2$	Average of the squared of the momentum	$kg^2 eV^2$
$|M_{ee}|^2$	The matrix element of the electron-electron interaction	s^2/kg^2
$|M_o|^2$	The transition matrix element	kg. eV
M_{TE}	Average of the squared momentum matrix	$kg^2 eV^2$

	element for the TE mode	
M_{TM}	Average of the squared momentum matrix element for the TM mode	$kg^2 eV^2$
$\langle M^2 \rangle_{hh,TE}$	The squared momentum matrix element of the electron - heavy hole for the TE mode	$kg^2 eV^2$
$\langle M^2 \rangle_{lh,TE}$	The squared momentum matrix element of the electron -light hole for the TE mode	$kg^2 eV^2$
$\langle M^2 \rangle_{hh,TM}$	The squared momentum matrix element of the electron - heavy hole for the TM mode	$kg^2 eV^2$
$\langle M^2 \rangle_{lh,TM}$	The squared momentum matrix element of the electron - light hole for the TM mode	$kg^2 eV^2$
Δ_o	Split off energy	eV
A, B	Constants	none
R_{rad}	Radiative recombination coefficient	$cm^3 . s^{-1}$
R_D	Defect recombination rate	$s^{-1} cm^{-3}$
A_D	Monomolecular recombination coefficient	s^{-1}
R_{Aug}	Auger recombination rate	$s^{-1} cm^{-3}$
C_n	Auger coefficient electron	$cm^6 . s^{-1}$
C_p	Auger coefficient hole	$cm^6 . s^{-1}$
τ_A	Auger carrier lifetime	s^{-1}
C_{Aug}	Auger recombination coefficient	$cm^6 . s^{-1}$
f_c, f_v	the Fermi Dirac distribution function for electron and hole	non
E_{fc}, E_{fv}	Quasi Fermi levels in the conduction and valence bands	eV
E_e, E_h	Electron and hole energies	eV
E_c, E_v	Above the conduction band energy and below the valence band energy	eV
N_c, N_v	Effective density of states for electrons and holes	cm^{-3}
$D_r(E)$	The density of allowed transition between two bands	cm^{-3}
M	Momentum matrix element	kg eV

E_a	Activation energy	eV
J_{th}	Threshold current density	A/cm^2
N_{th}	Threshold carrier density	cm^{-3}
N_{tr}	Transparency carrier density	cm^{-3}
I_{th}	Threshold Current	mA
g_{th}	Threshold gain	cm^{-1}
g_o	Gain coefficient	cm^{-1}
T	Temperature	K
λ	Wavelength	nm
c	Velocity light	m/s
D	Normalized thickness of the active region	none
b	Barrier width	nm
Γ^{SQW}	Single quantum well optical confinement factor	none
Γ^{MQW}	Multi quantum well optical confinement factor	none
N_w	Number of well	none
N_b	Number of barrier	none
α_i	Internal Loss	cm^{-1}
α_m	Mirror loss	cm^{-1}
k_b	Boltzmann's constant	eV/K
x	Mole fraction	none
E_f	Fermi energy	eV
E_t	Total energy	eV
v	The velocity wave	m/s
τ_{rec}	Recombination Lifetime	s
τ_r	Radaitive lifetime	s
τ_D	Defect lifetime	s
T_o	Temperature constant	K
n_{rw}	Refractive index of active region	none
n_{rc}	Refractive index of cladding	none
n_{γ}	Average index refraction	none

CHAPTER ONE

Introduction and LITERATURE REVIEW

1.1 Introduction

The technology of semiconductor lasers and since the invention of laser in the sixties of the last century to the present time has developed a tremendous development. In fact, laser, in various forms, entered in almost all life fields; scientific, military, medical, industrial and agricultural, due to its unique properties such as the coherency and peak powers.

Semiconductor lasers (SLs) are used in many applications such as communications and image transmission, compact disc (CD) player, bar-code readers, computer interconnects, network, cable TV signal transmission, laser printers and many military applications [1]. The semiconductor laser is a main element of optical communication systems. Because of its suitability include compact size [2, 3], high reliability, suitable wavelength range [2] and the fact that its power can be directly modulated through variation of the injection current [3].

The semiconductor laser and light emitting diode (LED) belong to the luminescent device family [4]. Semiconductor laser is emitting coherent light generated by stimulated emission process. The process of light emission in semiconductor laser is more complex than that in light emitting diodes (LEDs), where light produced in light emitting diodes by a spontaneous emission process. LEDs the widely used in various types of systems and equipment, the emitting from blue to red light. LED has used in optical fiber communication systems, remote controllers, data links, etc. [5].

In recent years, small dimensional semiconductor laser systems have generated great interest. This system called nanostructure semiconductor laser, where small dimensional system refers to the materials that show unusual structure because of the confinement of electrons to less than three directions from their ordinary bulk materials. Depending on how many dimensions lay within the range of nanoscale, generally speaks of two dimension (2D) such as quantum well (QW), one dimension (1D) such as

quantum wire (QWR) and zero dimension (0D) such as quantum dot (QD) [6]. The quantum confinement occurs when one or more of the dimensions of a nanocrystal are made very small so that these physical dimensions approach the size of an exciton in bulk crystal. Quantum confinement is defined as the physical size of a structure is nearly equal to that of the normal electron orbit [7].

In this chapter, explain Fundamental of Laser, Laser Diode, Structures of Laser Diode (homostructure and heterostructure lasers), semiconductor nanostructure with classification, quantum well lasers, density of states of quantum well, optical transition (direct and in direct band gap), III-V semiconductor laser materials, the literature survey, and the aim of this work .

1.2 Fundamental of Laser

1.2.1 Absorption, Spontaneous Emission and Stimulated Emission

The figure (1.1) shows absorption, spontaneous emission and stimulated emission. Figure (1.1a) illustrates the spontaneous emission where the emission photon is created by recombination of electrons-holes pairs and photons are random in phase, direction, and time resulting in incoherent light. This emission is the process in LEDs [8]. Figure (1.1b) shows absorption process that is the electron transfer from lower energy level to a higher energy level through absorption the energy of the incident light. Also called as the induced absorption, due to that transition is induced through the incident light. Figure (1.1c) shows stimulated emission which is the incident light leads to radiative transition electron excited, and light emitted due to the stimulated emission which has the same phase, wavelength and direction as the incident light. Therefore, the light generated by stimulated emission is coherent, highly monochromatic and direction. The incident photon in the stimulated emission generates two photons, one is the same incident photon, and the other is an

emitted photon due to the stimulated emission. This process works to amplify the incident light [9].

(a)   (b)   (c)
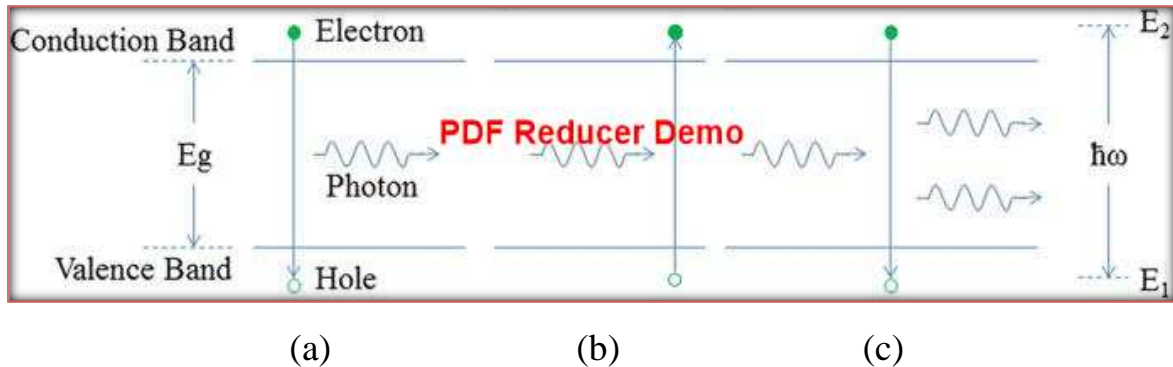
Figure (1-1): Three kinds of radiative band to band transition in semiconductor, a) Spontaneous emission b) absorption c) stimulated emission [8].

1.2.2 Population Inversion

The population inversion arises when the number of electrons in the upper energy level exceeds the number of electrons in the lower energy level. This also the rate of stimulated emission is higher than the absorption rate. Population inversion in semiconductor happen when the number of electrons in the conduction band (CB) increases and the number of electrons in the valence band (VB) decreases and this is done by forward biasing the p-n junction. Once the population inversion is achieved, the rate of stimulated emission must be increased beyond that of the spontaneous emission and to do this is required optical feedback [10].

1.2.3 Elements of Lasers

Laser is an acronym for light amplification by stimulated emission of radiation [11, 12]. A laser consists of three elements are active medium, pumping source and optical resonator as shown in figure (1-2). The active medium consists from group of the atoms, molecules or ions as (solid, liquid or gas) .The pumping source provides population inversion between a pair from energy levels in the atomic system and turn the light beam input can be

amplified through stimulated emission [11], can be a chemical reaction, a high voltage discharge, diode, flash lamp another laser. The optical resonator consists of cavity contains on lasing medium, with two parallel mirrors on both sides. One completely mirror reflective and other partially reflective mirror, and allows some of the light to leave the cavity to produce the laser beam output this is called the output coupler [12].The reflectivity of the mirror R is defined as the fraction of the incident intensity reflected by the mirror and can be given by the simplified equation [10]

$$R = \frac{(n_r - n_{air})^2}{(n_r + n_{air})^2}$$ (1-1)

n_r is the refractive index of the laser medium and n_{air} is the refractive index of the air equal 1.
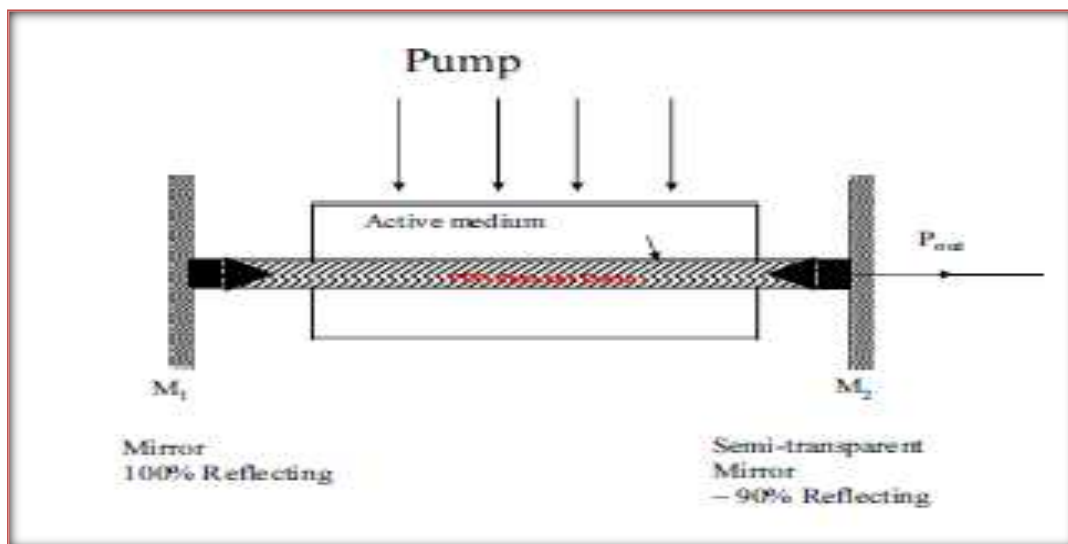
Figure (1-2): The elements of laser [11].

1.3 Laser Diode (LD)

Laser Diode also known as the semiconductor lasers [13]. The structure of semiconductor lasers is based on the p-n junction of the semiconductor materials and the oscillation of laser is realized by the emission of light due to the recombination of electrons in conduction band with holes in valence band [14]. There are three processes of band to band transition which are

4

absorption, spontaneous emission and stimulated emissions. In laser diodes (LDs), the stable laser beams are produced when three conditions are satisfied. There conditions are the optical gain, population inversion and the stable laser oscillation [8].

A main characteristic of a laser diode is the light current curve. Figure (1-3) shows the output optical power as a function of the pump current. The more linear is this curve, or the larger is its slope, or the closer is the starting point of the curve to the origin, the better is the semiconductor laser. The current density at the starter of lasing is called the threshold current density (J_{th}). The lower (J_{th}) is the higher output optical power at a given injection current density. The threshold current density dependent on temperature can be experimentally termed by an exponential function, where T_0 is the characteristic temperature. The higher T_0 is the temperature stability of J_{th}. Lowering J_{th} and improving its temperature stability have been important objects in the development of laser diodes [15].
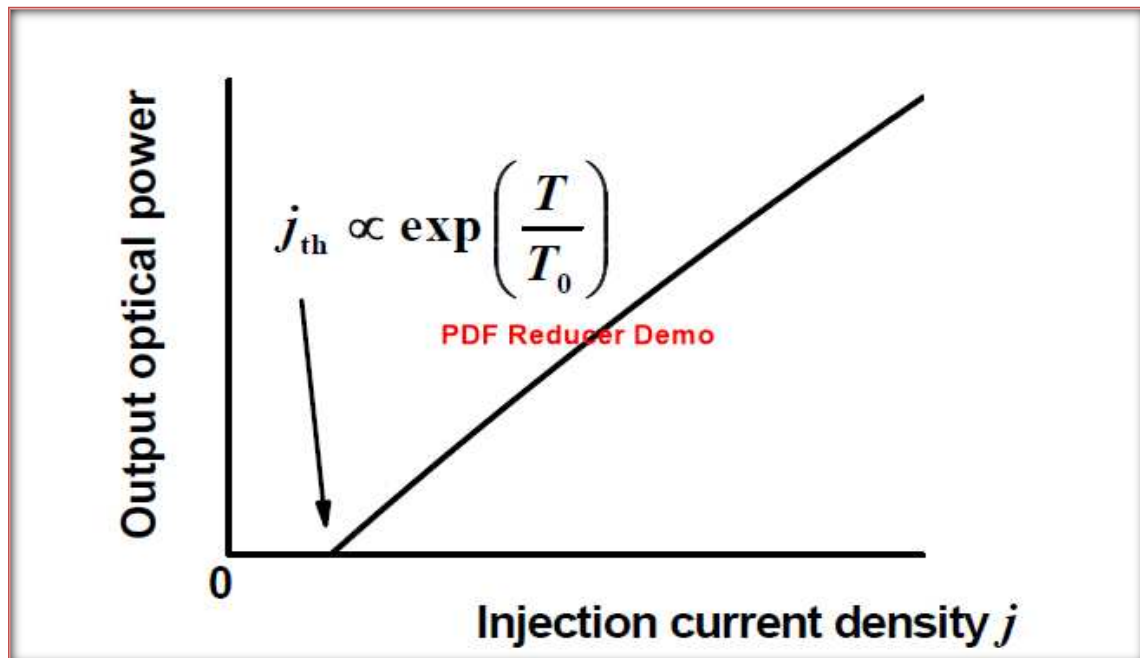
Figure (1-3): Light current curve of a semiconductor lasers [15].

1.3.1 p-n Junction

PN junction is formed in a single crystal of semiconductor through making one end of the crystal p-type by doping with acceptor atoms and the other end making n-type by doping with donor atoms. Meeting area p- type and n- type is the junction [16].

1.3.1.1 The Junction at Zero Bias

If assume that no voltage (V) is applied through the p-n junction .In thermal equilibrium figure (1-4) shows the energy band diagram for the p-n junction. The conduction and valence band energies must bend as we go through the space charge region, since the relative position of the conduction and valence bands with respect to the Fermi energy changes between p and n regions.

Electrons in conduction band of the n region see a potential barrier (V_B) in trying to move into the conduction band of the p region. The built in potential barrier keeps equilibrium between majority carrier electrons in the n region and minority carrier electrons in the p region, and also between majority carrier holes in the p region and minority carrier holes in the n region. The Fermi level is constant through the entire system [17].
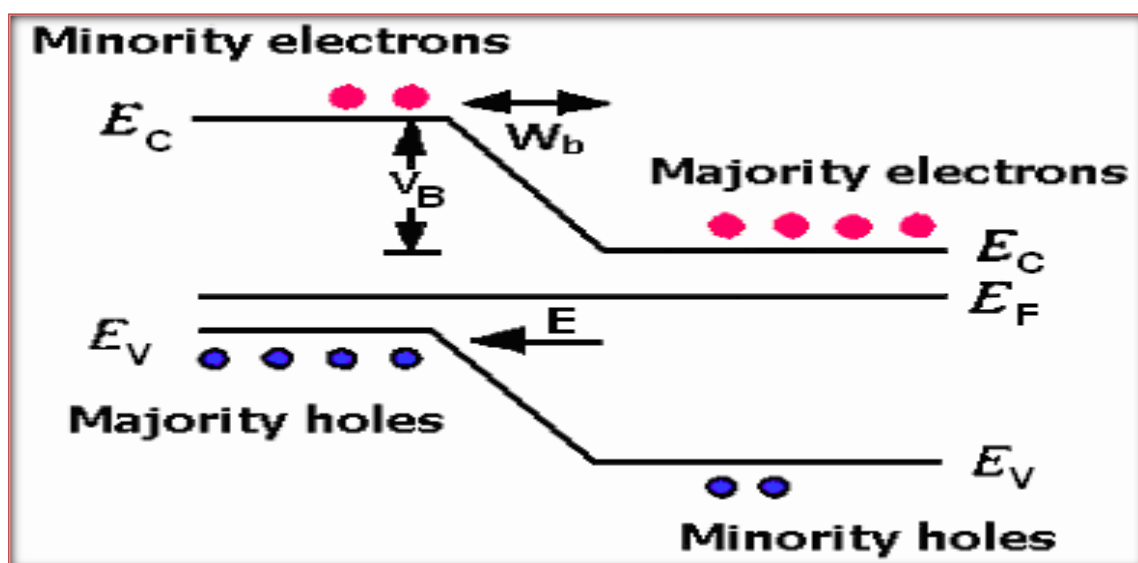
Figure (1-4): The energy band diagram for the p-n junction in thermal equilibrium [16].

The depletion region is defined a region that lack of carrier of certain thickness is made at both side of the junction, as shown fig (1- 5) [16].
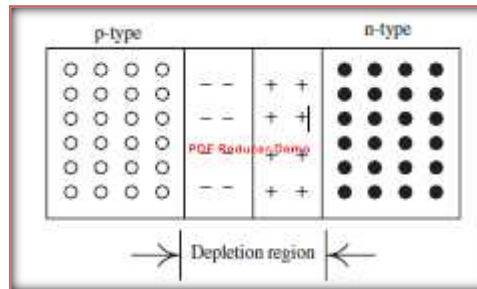
Figure (1-5): The depletion region [18].

1.3.1.2 The Junction under Forward Bias

When the applied voltage to the p-n junction (positive polarity applied to the p-side and negative to the n-side), the potential barrier across the junction will decrease to (V_B -*V*). In this case, the potential barrier for the majority carriers at the junction is reduced, and the depletion layer width is decreased, the current flow increases. Figure (1-6) shows the energy band diagram for a p-n junction under forward bias [19].

The Fermi levels in the valence band for the p-type E_{Fp} and in the conduction band for the n-type E_{Fn}, two Fermi levels become separated by ΔE= eV [20].
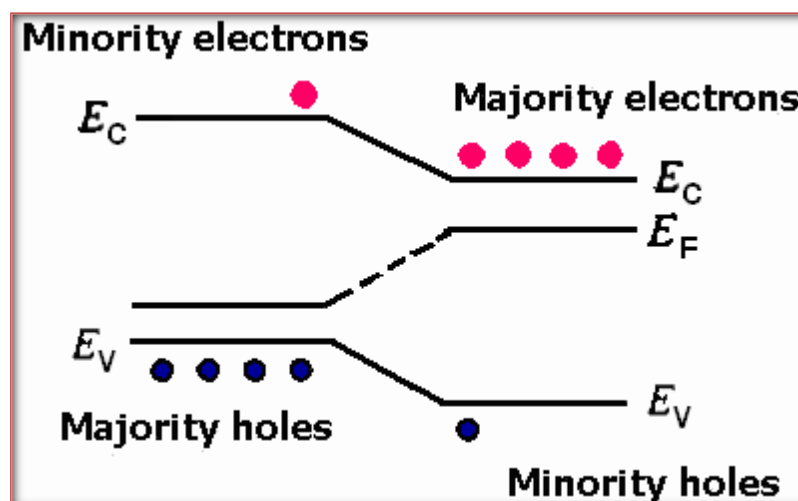
Figure (1-6): The energy band diagram for a p-n junction under forward bias [16].

1.4 Structures of Laser Diode

1.4.1 Homostructure Lasers

   Homostructure Lasers comprised from two layers made from the same material, generally GaAs. one layer of this structure doped with donor atoms material which it add extra electrons to the conduction band to create a n-type semiconductor, and the other layer doped with acceptor atoms material that generated holes in the valence band to create a p-type material. The two layers separated by the junction zone. This structure also called homojunction lasers [21]. Figure (1-7) shows the schematic of homojunction laser [22].
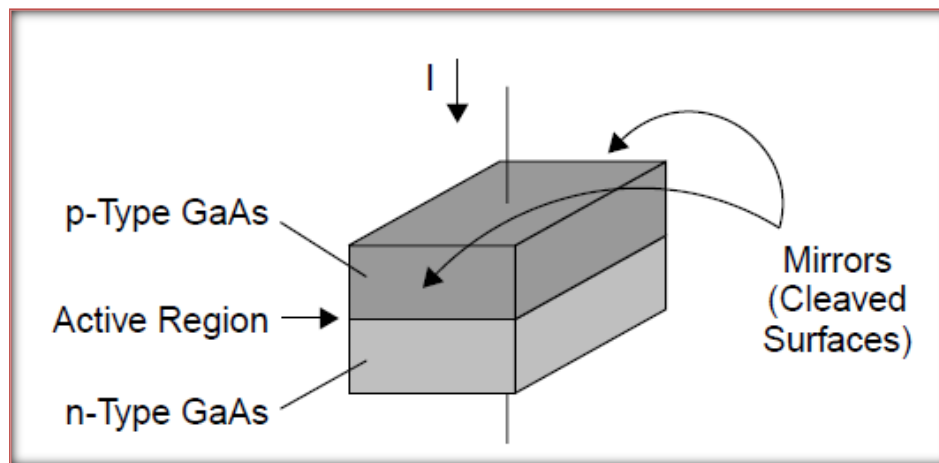
Figure (1-7): Show the schematic of homojunction laser [22].

   The index of refraction of a doped semiconductor depends on the particular dopant used. As well as the doping level. In a homojunction device, the p-n junction region is actually lightly doped p-type material, which creates a region with a higher index of refraction. The surrounding n-type material and more heavily doped than p-type material have a lower index of refraction than the junction region .The small index of refraction junction surrounded by the higher index of refraction material forms an optical waveguide structure that helps to confine the laser light to the active junction region. The total internal reflection material can happen when light travels from a high index of refraction. The disadvantage of homojunction lasers is that the efficiency is low and the threshold current density for laser operation is high [23].

1.4.2 Heterostructure Lasers

In this structure the junction arises between two semiconductors with different energy gap, they are called heterojunctions [24]. The heterostructure lasers are classified into two type's single heterostructure (SH) and double heterostructure (DH) lasers depending on whether the active region is surrounded by one or two cladding layers [25].Single heterostructure consists of only one heterojunction [26], figure (1-8) show single heterojunction laser [27], and double heterojunction consists of two heterojunction [26].
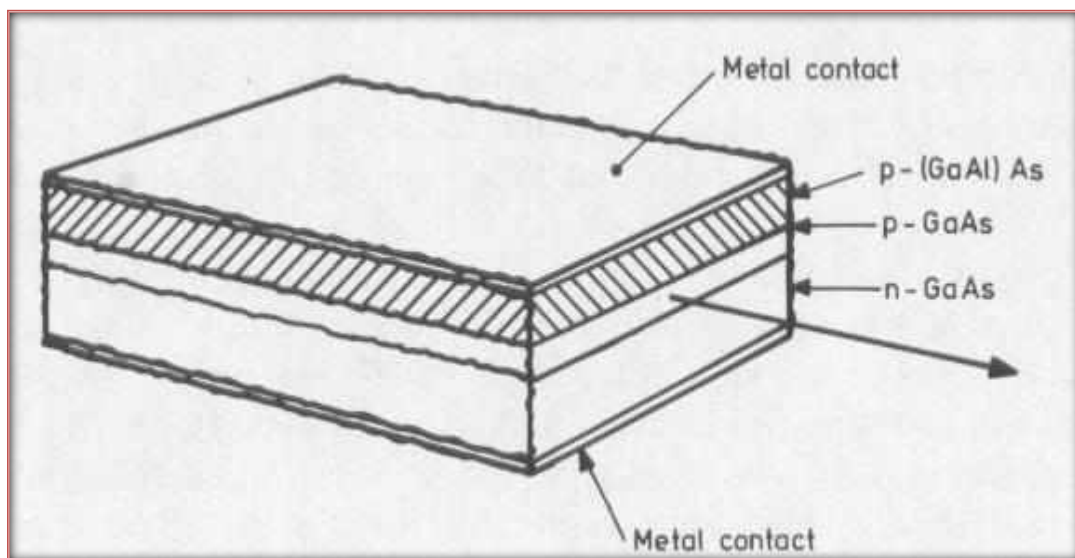
Figure (1-8): Show single heterojunction laser [27].

Double heterostructure laser makes use of a small band gap material which is sandwiched between two high band gap material layers. GaAs with AlGaAs is one commonly used pair of materials. The feature of a DH laser over a homojunction laser is that the area where free electrons and holes are simultaneously is confined to the thin middle layer [28]. Figure (1-9) shows the structure double heterostructure laser [29].
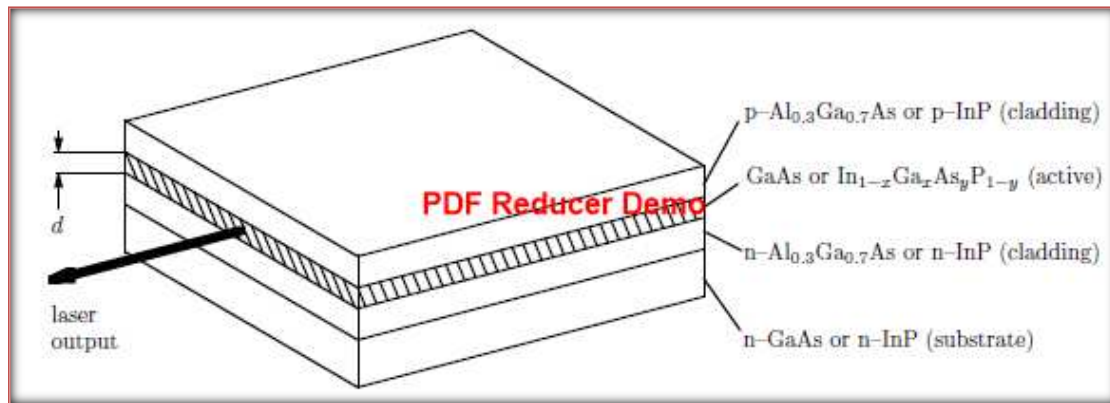
Figure (1-9): Show the structure of a double-heterostructure laser [29].

The band gap difference between the active layer and the cladding layer confine electrons and holes to the active layer for more effective recombination. Also the cladding layers with high band gap energy have lower refractive index compared to the active region. This refractive index difference confines the optical mode very close to the active layer. This refractive index difference achieves more optical gain, then the internal losses decrease. Figure (1-10) shows the charge carrier and the optical mode confinement in the active region [25].

Heterostructure based electron devices are widely used in many areas of human activity. life without telecommunication systems utilizing double heterostructure (DH) lasers, heterostructure bipolar transistors, heterostructure light emitting diodes, or without the low noise high electron mobility transistors (HEMTs) for high frequency devices, including satellite television system is scarcely conceivable. The (DH) laser is now found in virtually every house as part of the compact disc (CD) player. Solar cells incorporating heterostructures are used extensively in both space and terrestrial programs [30].
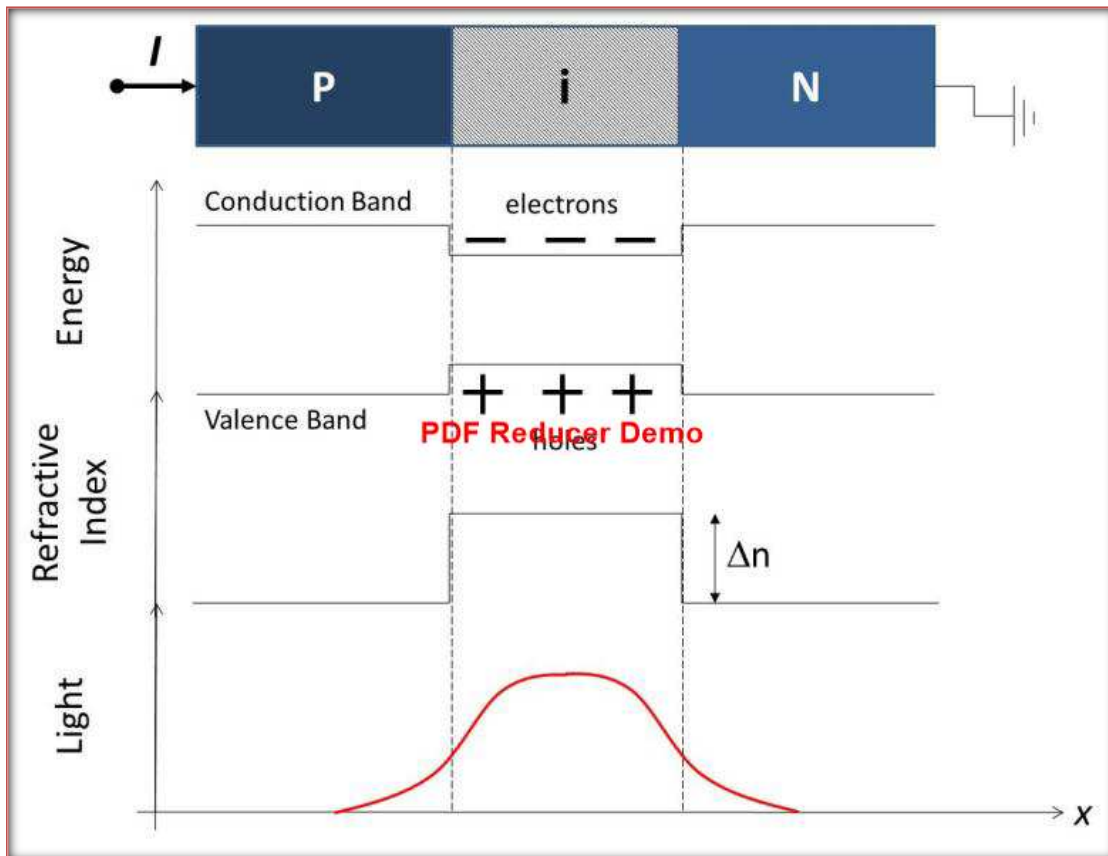
Figure (1-10): Double heterostructure carrier and optical mode confinement from top to bottom: material structure, energy diagram, refractive index profile and the optical mode profile [25].

1.5 Semiconductor Nanostructure

The low dimensional semiconductor structures have extensive areas of higher research activity, they have promising potential applications in such fields as nonlinear optics, light emitting materials, and optoelectronic devices, as well as new applications that have been opened up in optical communications. Nanostructure is defined as having at minimum one dimension between 1 and 100 nm [31].

The nanostructure dimensions are similar to the de Broglie wavelength of the electron, their properties related for nanoelectronic applications are described by quantum mechanics, which is in contradiction with classical microelectronics. Nanostructures can be formed out of different materials,

either metals, dielectrics, or semiconductors [32], nanostructures produce from new fabrication technology where size control, shape control and uniformity can be kept within accuracy of nanometer scale [31].

1.5.1 Classification of Semiconductor Nanostructure

There are many classifications for semiconductor nanostructure materials which dependent on the method of their manufacture, on their chemical composition, or on their dimensionality. The most common classification of semiconductor nanostructures is on their dimensionality. In fact, this classification, is assumed according to the number of dimensions L_x, L_y, L_z, which is larger than the characteristic length, L_0. The characteristic length is defined as the depiction of the electrons behavior in semiconductor materials [31].Thus, there are many L_0, such as de Broglie wavelength, diffusion length, and mean free path [33], or Bohr radius [34]. Then the characteristic lengths differ from material to another [35]. This classification as the following:

1.5.1.1 Zero Dimension Nanostructure (0D)

Zero dimension is a structure capable of confining electrons in all three dimensions [36], where $L_0 > L_x, L_y, L_z$ [31], thus letting zero dimensions (0D) in their degrees of freedom, also known as a quantum box or quantum dot [36].

The total energy is the sum of three discrete components is given by [36, 37]

$$E_t = E_{n_x} + E_{n_y} + E_{n_z} \tag{1-2}$$

$$E_{n_x} = \frac{n_x^2 \hbar^2 \pi^2}{2m_e^* L_x^2} \tag{1-3}$$

$$E_{n_y} = \frac{n_y^2 \hbar^2 \pi^2}{2m_e^* L_y^2} \tag{1-4}$$

$$E_{n_z} = \frac{n_z^2 \hbar^2 \pi^2}{2m_e^* L_z^2} \tag{1-5}$$

thus

$$E_t = \frac{\hbar^2 \pi^2}{2\,m_e^*} \left(\frac{n_x^2}{L_x^2} + \frac{n_y^2}{L_y^2} + \frac{n_z^2}{L_z^2} \right)$$
(1-6)

Where E_{n_x, n_y, n_z} are the quantized energy levels, m_e^* is the electron effective mass, n_x, n_y, n_z are the number of states, $\hbar$ is the Planck constant divided by 2π ($h/2\pi$).

1.5.1.2 One Dimension Nanostructure (1D)

One dimension is formed when the motion of electron in the conduction band is confined in two directions (y, z), while it remains free to move in the remaining direction (x), also known as a quantum wire [36], where $L_x > L_0 > L_y, L_z$ [31].

The total energy is the sum of three components is given by [36, 37]

$$E_t = \frac{\hbar^2 k_x^2}{2\,m_e^*} + E_{n_y} + E_{n_z}$$
(1-7)

Where the first term indicates to the kinetic energy of the electrons in x direction.

1.5.1.3 Two Dimension Nanostructure (2D)

Two dimension is formed when the motion of electrons is confined in one direction (z), while it remains free to move in the other two directions (x, y), also known as a quantum well [36], where $L_x, L_y > L_0 > L_z$ [31].

The total energy spectrum for an electron in a quantum well is given by [36, 37]

$$E_t = \frac{\hbar^2 (k_x^2 + k_y^2)}{2\,m_e^*} + E_{n_z}$$
(1-8)

1.5.1.4Three Dimensional Nanostructure (3D)

The three dimensional, there are three degree of freedom directions and zero confined directions, also known as a bulk materials [38], where $L_0 < L_x$, L_y, L_z [31].

The total energy in three dimensions is given by [37]

$$E_t = \frac{\hbar^2 (k_x^2 + k_y^2 + k_z^2)}{2\, m_e^*} \qquad\qquad (1\text{-}9)$$

1.6 Quantum Well Laser (QW)

A quantum well is a special type of heterostructure in which one thin well layer is surrounded by two barrier layers [39]. The active region of the quantum well laser structure is a narrow layer a quantum confinement occurs, according to quantum mechanics. The wavelength of the emitted light for QW laser is determined by the active region width rather than just the band gap of the material of which the device is realized [40]. Figure (1-11) shows the single quantum well and its transition energies [41]. The potential wells defined as the low energy regions for the electrons in the conduction band and the holes in the valence band. Also note that in figure (1-11), the vertical line shows that the energies of carriers decrease with an increase in the height of the vertical line. Potential well is called quantum well, when the well width L_z is lower than several tens of nanometers. The band gaps energy of barrier layers ($E_{g(b)}$) are higher than those of well ($E_{g(w)}$) [9]. The band gap energy well is not the same as the emission wavelength, E_{c1}-$E_{hh(lh)}$ [41]. Band offsets in the interfaces of the quantum well and the barriers, is the energy differences in the conduction band ΔE_c and the valence bands ΔE_c [9].
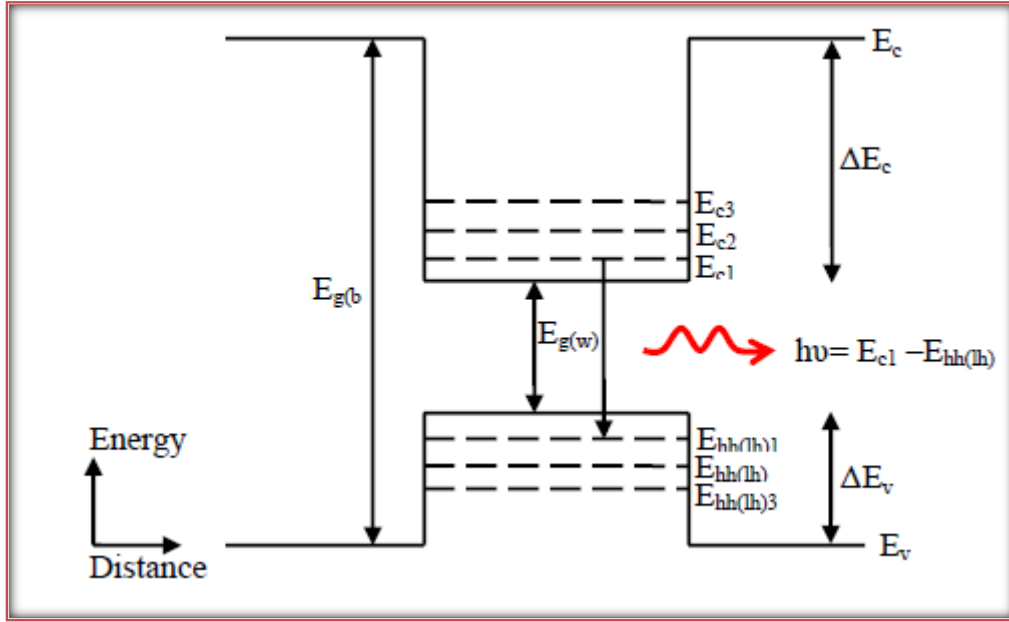
Figure (1-11): The quantum well structure [41].

The electrons motion in the quantum well layer is confined in the growth direction when the thickness of the quantum well layer is in the order of the de Broglie wavelength (λ=h/p), where h is the Planck constant and p is the momentum [42].

The variance between the DH laser and the QW laser is the thickness of the active region. Typical thickness of the active layer for the DH is (50-300) nm whereas the thickness of the QW is just (5-10 nm) [8], is much smaller from the wavelength of IR radiation [43]. A semiconductor quantum well is not on infinite potential well because the heights of the energy steps at the DH junctions are finite. However taking the energy quantization of an infinite potential well as an approximation, we can express the band edges of the quantized conduction and valence subbands respectively as given

$$E_c^{QW} = E_c + \frac{n^2\pi^2\hbar^2}{2m_e^*L_z^2} \qquad\qquad (1\text{-}10)$$

$$E_v^{QW} = E_v - \frac{n^2\pi^2\hbar^2}{2m_h^*L_z^2} \qquad\qquad (1\text{-}11)$$

Where n = 1, 2, 3… the number of quantized subbands for electrons and holes depend on the heights of the potential, m_h^* is the hole effective mass, L_z is the well width [26].

The energy band gap can be written [41]

$$E_g = \frac{h\,c}{\lambda} \tag{1-12}$$

Where c is the velocity light and λ is the wavelength.

Photon energy required for transition between conduction subband and valence subband is [26]

$$h\nu = E_g + \frac{n^2\pi^2\hbar^2}{2m_e^*L_z^2} + \frac{n^2\pi^2\hbar^2}{2m_h^*L_z^2} \tag{1-13}$$

The energy band gap in the QW can be written

$$E_g^{QW} = E_g + \frac{n^2\pi^2\hbar^2}{2m_e^*L_z^2} + \frac{n^2\pi^2\hbar^2}{2m_h^*L_z^2} \tag{1-14}$$

Quantum well laser is classified into two types single and multiple quantum well lasers

1.6.1 Single Quantum Well (SQW)

Single quantum well is the structure of the ultra-thin layer with narrow band gap is inlayed into the central of the two types of material with wide band gap [8]. Figure (1-12a) shows SQW active layer, the optical confinement factor (Γ) is small because the well width L_z is as thin as 10 nm or lower. The threshold current density J_{th} is large because the small optical confinement factor. Figure (1-12b) shows separate confinement heterostructure (SCH), which has two energy steps, is able to obtain a large optical confinement factor in the SQW active layer. The materials which used for laser diodes have the reverse proportional of refractive index with the band gap. By the distribution of the refractive index is determined the external potential confines light in the QW active layer, the inner potential confines

the carriers by the energy barriers. This is called (SCH) since the potentials to confine light photon and the carriers are separate. Figure (1-12c) shows a graded index SCH (GRIN-SCH) whose refractive index and potential distributions in the external of the active layer are parabolic. The optical confinement factor of a GRIN-SCH is relational to L_z and the optical confinement factor of an SQW is proportional to L_z^2, when the well width L_z is small. The optical confinement factor of the GRIN-SCH is higher than of the SQW, when active layer is thin [9].

1.6.2 Multi quantum well (MQW)

   Multi quantum well is the structure of the ultra-thin layers with narrow band gap and broad band gap are placed alternately on the chip [8]. The layers separating the active regions are called barrier layers [44]. Figure (1-12d) shows MQW; the efficiency of carrier injection decreases with propagation of the carriers, however due to the energy barriers between the neighboring QW active layers. Therefore it is hard to achieve uniform carrier distribution all over the MQW active layers [9].

   Modified multi quantum well which that the band gap energy of the barrier layer differs from the cladding layer in a MQW device [44] as shown in fig (1- 12e) [9], it has demonstrated the superior characteristics of MQW devices over conventional DH lasers in relation to lower threshold currents, higher modulation speeds, narrower line widths, lower frequency chirp and less temperature dependence .The confinement of the optical mode is obtained in MQW lasers in comparison with SQW lasers [44].
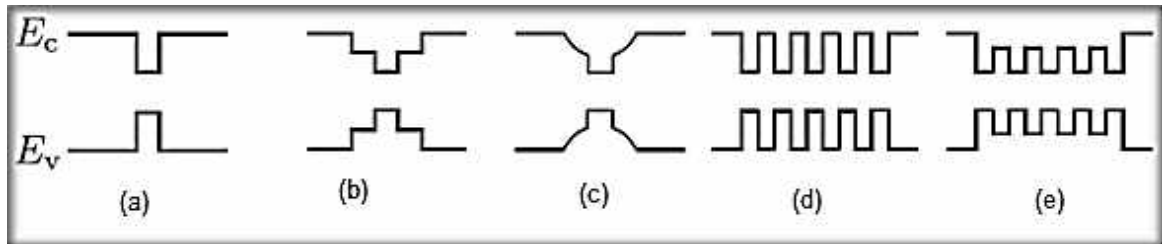
Figure (1-12): Show the types of quantum well structure: a) SQW, b) SCH, C) GRIN -
SCH, d) MQW, e) modified MQW [9]

1.7 Optical transition

Semiconductor lasers have been made from several different semiconductor materials. The chief aim for investigating the use of different materials is to extend the range of possible wavelengths [27]. A semiconductor is classified into two types are direct and indirect band gap semiconductors, according to the energy band distribution in wavenumber space. Figure (1-13a) shows the direct band gap such as Si and Ge where the top of the valence band and the bottom of the conduction band have the same value of wavenumber (k). In this case, exiting electron and electron-hole recombination are direct processes which required only photon. Indirect band gap semiconductor such as GaAs, figure (1-13b) illustrates that the variance in wavenumber value between the top of the valence band and the bottom of the conduction band, the emission process required extra variation of crystal momentum (phonon). But photons cannot carry crystal momentum, thus, the emission efficiency of direct band gap semiconductors is much higher than that of indirect band gap semiconductors [45]. Generally, all of these semiconductor materials are direct band gap except for some of the alloy composition [4].
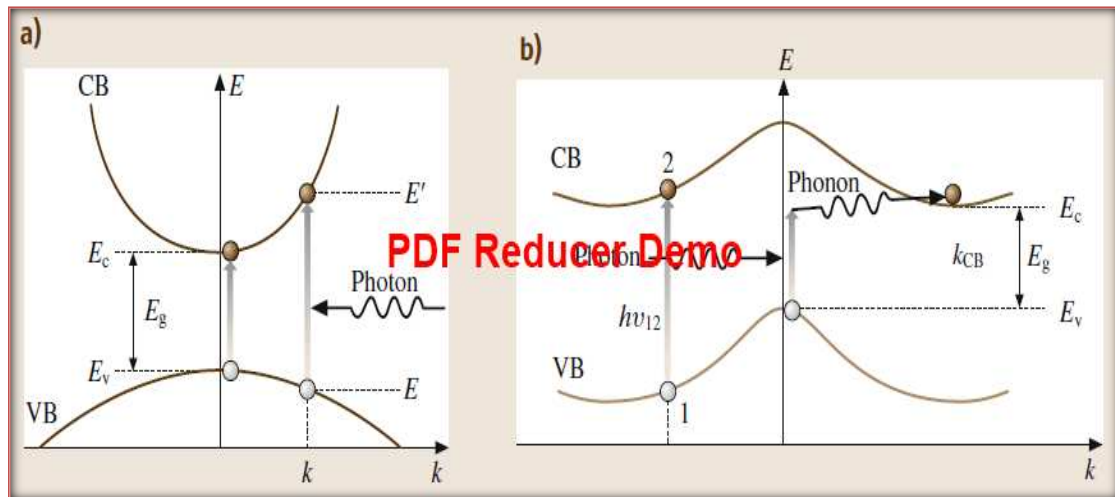
Figure (1-13): The band energy diagram direct and indirect semiconductors [45].

1.8 Density of States (DOS)

The density of states (DOS) function describes the number of states that are available in a system and is important to determining the carrier concentration and energy carriers' distributions within a semiconductor [46]. DOS (E) can be defined as the number of a states per unit energy per unit volume, can be express through the following equation

$$\text{DOS (E)} = \frac{\partial N}{\partial E} \qquad \qquad (1\text{-}15)$$

1.8.1 Bulk Density of States

The unit cell volume in the k- space full by one state is

$$V_k = k_x \, k_y \, k_z = \frac{(2\pi)^3}{L^3}$$

$$k_x = \frac{2\pi}{L_x}, \;\; k_y = \frac{2\pi}{L_y} \;, k_z = \frac{2\pi}{L_z}$$

Where $L_x = L_y = L_z = L$

N The total number of states is equal to the degeneracy times the volume of the sphere in k-space divided by the volume occupied by one state and divided again by the volume of real space such that

$$N = 2 \frac{4\pi k^3}{3} \frac{1}{(\frac{2\pi}{L})^3} \frac{1}{V} = \frac{2}{3} \frac{4\pi k^3}{(2\pi)^3} \qquad (1\text{-}16)$$

Where we assume $V=L^3$, 2 is the degeneracy for spin up and spin down. The density of states can be written as

$$DOS\ (E) = \frac{\partial N}{\partial k} \frac{\partial k}{\partial E} \qquad (1\text{-}17)$$

$$\frac{\partial N}{\partial k} = 2 \frac{4\pi k^2}{(2\pi)^3} \qquad (1\text{-}18)$$

The energy of the electrons is

$$E = \frac{\hbar^2 k^2}{2\,m_e^*} \qquad (1\text{-}19)$$

$$\frac{\partial k}{\partial E} = (\frac{2m_e^*}{\hbar^2})^{\frac{1}{2}} \frac{1}{2\sqrt{E}} \qquad (1\text{-}20)$$

Substituting equation (1-18) to (1-20) into equation (1-17)

$$DOS\ (E) = \frac{1}{2\pi^2} (\frac{2m_e^*}{\hbar^2})^{\frac{3}{2}} \sqrt{E} \qquad (1\text{-}21)$$

Figure (1-14) show a plot of g (E) as a function of energy [38], the density of states function depend on square root energy [38, 47].
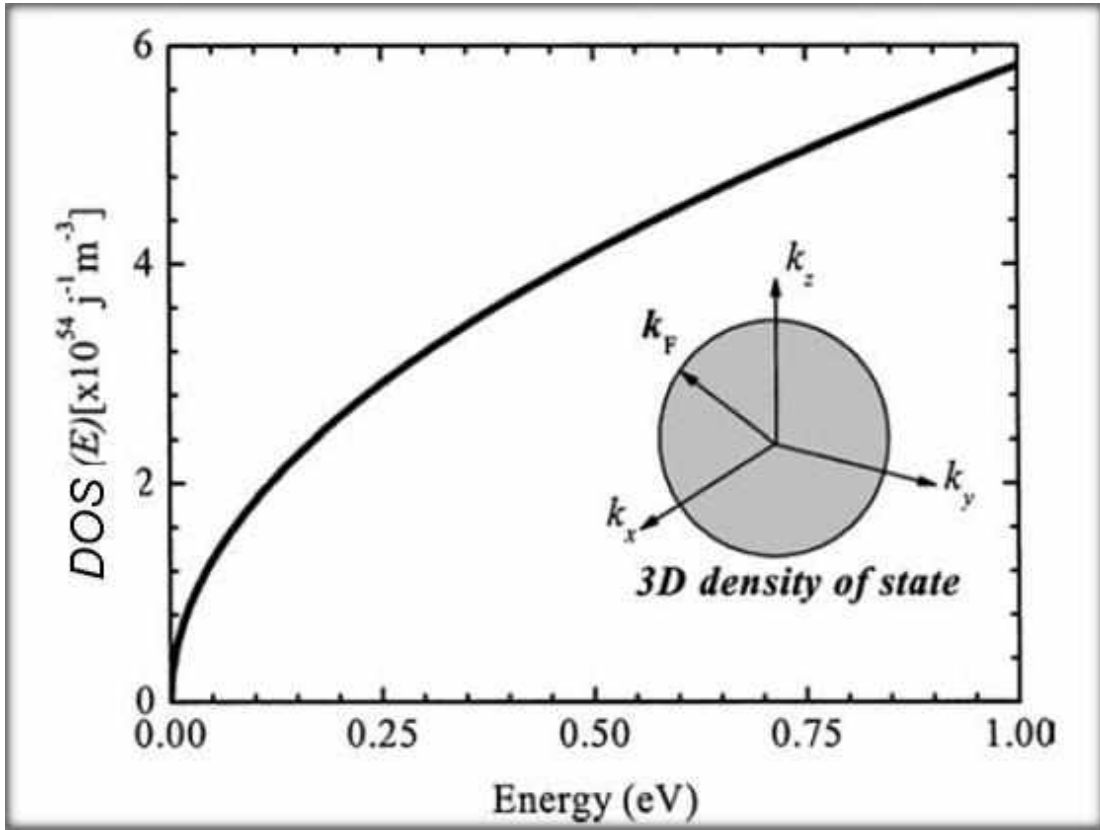
Figure (1-14): A plot of DOS (E) as a function of energy [38].

1.8.2 Quantum Well Density of States

The density of states in a quantum well structure is limited to the k_x k_y plane displayed figure (1-15).The total number of states per unit cross-sectional area, N^{2D}, is given by the area in k space divided by the area in real space and divided by the area of the unit cell in k- space:

$$N^{2D} = 2\pi k^2 \ \frac{1}{(\frac{2\pi}{L})^2} \ \frac{1}{L^2} \ = 2 \ \frac{\pi k^2}{(2\pi)^2} \qquad (1\text{-}22)$$

Where factor 2 is Indicates to a spin degeneracy of electrons, L^2 is the square area in real space, and $\frac{2\pi}{L}$ is the two dimensional primitive unit cells in k space.

The density of state can be written

$$DOS^{2D} (E) = \frac{\partial N}{\partial E} \ = \frac{\partial N}{\partial k} \frac{\partial k}{\partial E} \qquad (1\text{-}23)$$

$$\text{DOS}^{2D} (E) = \frac{k}{\pi} \left(\frac{2m_e^*}{\hbar^2}\right)^{\frac{1}{2}} \frac{1}{2\sqrt{E}} = \frac{m_e^*}{\pi \hbar^2} \qquad (1\text{-}24)$$

The density of states at a particular energy is the totality over all subbands less than the certain energy

$$\text{DOS}^{2D} (E) = \sum_{j=1}^{n} \frac{m_e^*}{\pi\hbar^2} Y(E - E_i) \qquad (1\text{-}25)$$

Where n is the total number of confined subbands less than the certain energy, Y is a step function defined as

$$Y \ (E\text{-}E_i) = \begin{cases} 1 \, for \ E > E_i \\ 0 \, for \ E < E_i \end{cases} \qquad (1\text{-}26)$$

DOS is independent of the energy [38]. Figure (1-16) show the diagram of the transition of the typical quantum well in which heavy hole (hh) band and light hole (lh) band is involved which comes from splitting of degeneracy of valence band by electron – orbit interaction [37].
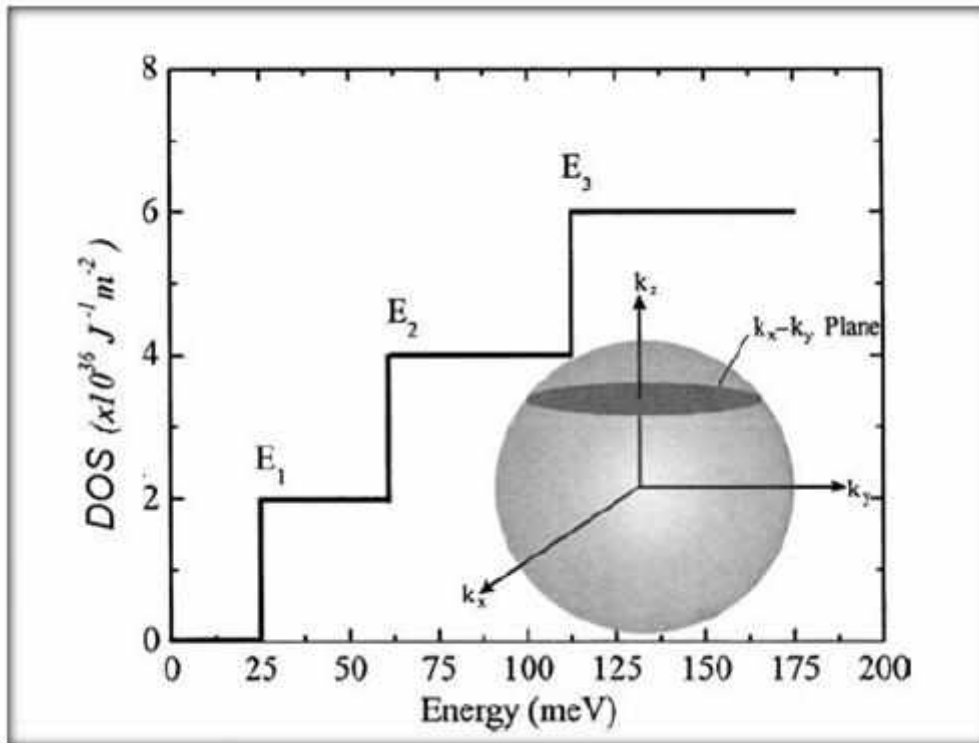
Figure (1-15): A plot the density of states as a function of energy in quantum well [38].
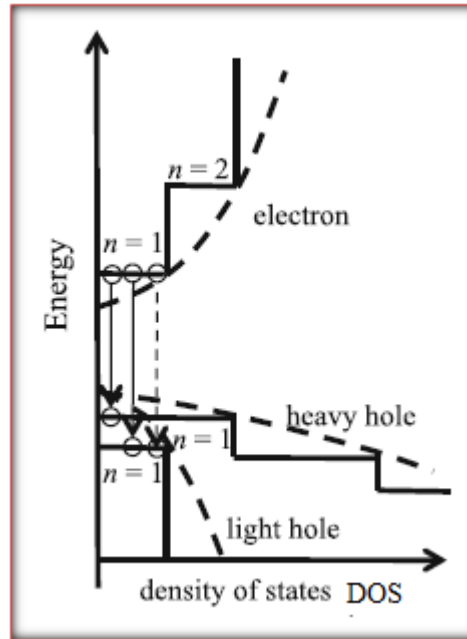
Figure (1-16): The diagram of the transition quantum well [37].

1.9 III-V Semiconductor Laser Materials

Composite semiconductors are crystalline solid state alloys formed from the mixture of two or more elements [48].It is composed of elements of group III and group V of the periodic table. The formation of the crystal structure must be binding the atoms together [41].Most semiconductor lasers are based on compounds of the III-V [27]. The advance in III-V nitride technology leading to the availability diodes is of blue laser diodes as a recent example [48]. Therefore we used AlGaN/GaN quantum well laser.

1.9.1GaN Material

Since 1997, by light emitting diode with semiconductor devices can be obtained the full visible spectrum. It is very important to develop the emitters of blue light because it is the last missing in the reconstruction of white light. GaN-based components are the most efficient in this field. These devices used instead of conventional lighting for domestic lighting and the roadside (traffic lights) due to their high reliability and their little energy consumption. As

well as the possibility which presented by nitrides and their alloys duo to their essential possessions to developed ultraviolet and blue lasers, permits the systems production to have playback of digital information and larger storage capacity, this capacity is times four [49]. GaN is a binary III-V direct band gap semiconductor usually used in bright light emitting diodes since the 1990s [50].Search began on GaN in the 60s and in 1971 was conducted a first blue LED based on GaN. The development of GaN was limited because failures in attempts to doping p and the poor quality of the material obtained. Recent research has led to a decent quality material, and in the development of doping p. These two performances have developed the light emitting diodes and lasers established on nitrides [49]. GaN is a promising semiconductor for high frequency, high temperature, high thermal conductivity, high carrier saturation velocity, high breakdown field, high power electric devices because its wide band gap [50], high chemical stability, very well mechanical and physical properties [49].

GaN has two types of the crystal structures are hexagonal wurtzite and cubic zinc structures as shown in figure (1-17). The crystal of a semiconductor compound contains both bonds covalent and ionic. The nitride semiconductors are usually strong iconicity. The most common structure of GaN crystal is the wurtzite structure and it is the most stable structure in thermodynamics steady state at room temperature and 1 atm. On the other hand the zinc blende structure is metastable structure. Usually the GaN is in form of hexagonal wurtzite structure, but in the certain case zinc blende structure is also exist. In normal condition in wurtzite structure is be III-V nitride material are more stable and representative. Therefore most of the GaN devices or researches are founded on the wurtzite GaN. Through its crystalline structure, the properties of GaN are determined directly [50].
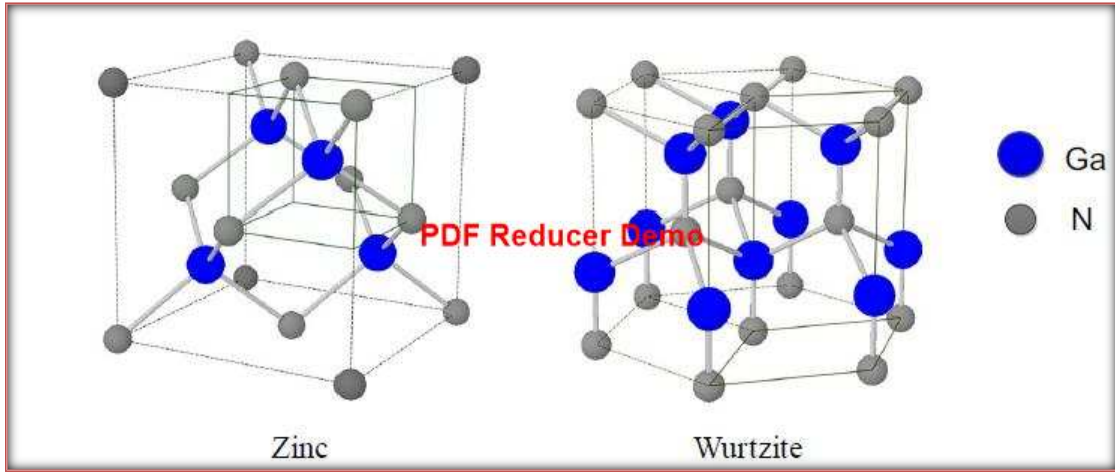
Figure (1-17): The crystal structure of GaN [50].

The temperature dependence of the energy gap equation as follows [49, 51]

$$E_g(T) = E_g(T = 0) - \frac{\alpha(x)T^2}{\beta(x)+T} \tag{1-27}$$

Where T is the temperature, $E_g(T = 0)$ the low band gaps of GaN = 3.507eV, α, β are constants equal (0.909 meV/K) and (830K) respectively in the wurtzite structure, x is the mole fraction.

1.9.2 AlGaN Material

AlGaN is the ternary alloys of wurtzite and zinc blened polytypes of GaN with AlN of a continuous alloy system with a wide range of band gap and a minor change in the lattice constant [52]. It is frequently used as the barrier material for nitride electronic and optoelectronic devices [51].

The energy band gap with mole fraction x can be written [53]

$$E_g(x) = (1 - x)E_{g\,(GaN)} + xE_{g\,(AlN)} - bx(1 - x) \tag{1-28}$$

Where b≈1 is the bowing parameter, $E_{g\,(GaN)}$ is the low temperature band gap value 3.5 eV, $E_{g\,(AlN)}$ is the low temperature band gap value 6.1 eV.

The energy band gap $Al_xGa_{1-x}N$ wurtzite structure also can be written as following [49]

$$E_g(x) = x^2 - 1.77\,x + 3.43 \tag{1-29}$$

Where α and β can be written as follows [53]

$$\alpha(x) = (1\text{-}x)\,\alpha_{(GaN)} + x\,\alpha_{(AlN)} - c\,x(1\text{-}x) \qquad (1\text{-}30)$$

$$\beta(x) = (1\text{-}x)\,\beta_{(GaN)} + x\,\beta_{(AlN)} - d\,x(1\text{-}x) \qquad (1\text{-}31)$$

The values $\alpha_{(GaN)}$, $\alpha_{(AlN)}$, $\beta_{(GaN)}$, $\beta_{(AlN)}$ is the 0.909 (meV/K), 1.799 (meV/K), 830 (K), 1462 (K) respectively and c =2.15 meV/K, d=1561.

The refractive index of AlGaN when $x < 0.3$ can be written [54]

$$n_{r\,(\text{AlGaN})} = 2.5067 \text{ - } 0.43x \qquad (1\text{-}32)$$

1.10 Literature Survey

In 1995 Hyo-Hoon Park and Byueng-su yoo using a periodic gain active structure in which three Quantum wells are introduced in two wavelength thick (2λ) cavity where obtain low threshold current densies with high light output powers for InGaAs /GaAs surface emitting lasers. Air post type devices with a diameter of (20-40) μm exhibit a threshold current density of (380-410) A/cm^2. The theoretical calculation of power performance and threshold into that the periodic gain structure has an advantage in achieving low threshold current density because of the high coupling efficiency between gain medium and optical field [55].

In 1996 W.J. Fan et al. the valence hole subbands, TE and TM mode optical gains, transparency carrier density, and radiative current density of the zinc–blende GaN / $Ga_{0.85}Al_{0.15}N$ strained quantum well. The compressive strain enhances the TE mode optical gain, and strongly depresses the TM mode optical gain. Even when the carrier density is as large as 10^9 cm^{-3}, there is no positive TM mode optical gain. The TE mode optical gain spectrum has a peak at around 3.26eV. The compressive strain overall reduces the transparency carrier density. The radiative current density is 0.53 kA/cm^2 for the zero optical gain [56].

In 1998 Y. C. Yeo, et al. studied the optical gain, DOS, and valence subband structures of wurtzite InGaN/GaN quantum wells. Where used the effective mass parameters InN and GaN resultant using the experimental pseudopotential method. As well as examined the compressive strain and the effects of quantum confinement by changing the width of well and mole fraction of in the well material. They obtained that the transparent current density (J_{tr}) for a SQW is 200 A/cm^2. In addition that a suitable combination of well width and number of QW structure should be nominated in optimizing the J_{th} in such MQW lasers [57]. In the same year Shuji Nakamura, et al. an InGaN multiquantum-well (MQW) structure laser diode was grown on an epitaxially laterally overgrown GaN on sapphire. The lowest threshold current densities between 1.2 and 2.8 kA/cm^2 were obtained when the number of InGaN well layers was two. The InGaN MQW LD was grown on a free-standing GaN substrate that was obtained by removing the sapphire substrate. The LDs with cleaved mirror facets showed on output power as high as 30mW under room temperature continuous wave (CW) operation. The stable fundamental transverse mode was observed by reducing the ridge width to a value as small as 2μm. The lifetime of the LDs at a constant output power of 5mW was about 160 h under CW operation at an ambient temperature of 50° C, due to a high threshold current density of 6 kA/cm^2 [58].

Sandra R.Selmic, et al. in 2001 designed uncooled multiple quantum well AlGaInAs -InP 1.3 m lasers for communication systems the complete design method for long wavelength strained quantum well. The method contains multiband effective mass theory and electromagnetic waveguide theory. For AlGaInAs-InP laser when temperature T=25°C the threshold current is I_{th}=12.5 mA, with slope efficiency of 0.43 W/A [59].

Nelson Tansu and Luke J. Mawst in 2005 applied the analysis presented to the current injection efficiency of 1200 nm emitting InGaAs and 1300 nm emitting InGaAsN quantum well lasers. The current injection efficiency of

InGaAsN quantum well lasers with big monomolecular recombination processes is shown to be less temperature sensitive [60].

K. Hild, et al (2006) studied the threshold current and its temperature dependence in GaAsSb – based quantum well edge emitting lasers for emission at 1.3μm. They found that the threshold current is dominated by nonradiative recombination accounting for more than 90% of the total threshold current density, at room temperature [61].

Yik.Khoon Ee, et al (2007) improved experimentally the light extraction efficiency of InGaN quantum wells light emitting diodes using SiO_2 polystyrene microspheres, leading 219% for InGaN quantum wells light emitting diodes which improve the output power [62].

Hongping Zhao. et al (2008) optical gain analysis exhibits significant improvement in the peak optical gain and differential gain for the strain compensated InGaN – AlGaN quantum well active regions for lasers emitting at 420–500 nm [63].

Harumasa Yoshida, et al. in 2009 the GaN/AlGaN MQW laser diodes lased at a peak wavelength ranging between 359.6 and 354.4 nm. A threshold current density of 8kA/cm^2, an output power as high as 80mW and a differential external quantum efficiency of 17.4% have been achieved. The AlGaN MQW laser diode lased at a peak wavelength down to 336 nm far beyond the GaN band gap. For the GaN/AlGaN MQW laser diodes, the modal gain coefficient and the optical internal loss are estimated to be 4.7± 0.6 cm kA^{-1} and 10.6± 2.7cm^{-1}, respectively. The results for the AlGaN based laser diodes grown on high quality AlGaN films presented have will be essential for the future development of laser diodes emitting much shorter wavelengths [64].

Dr. Azhar I. Hassan in 2010 the theoretical study of the dynamical behavior of single quantum well (SQW) GaAs/AlGaAs laser are studied theoretical with variable well widths L_z= (200, 150, 100, 75) A^o, at a band gap

discontinuity ΔE_c= 0.1 eV, show that the highest value of the peak modal gain g_{max}= 400cm^{-1}is achieved at L_z=75A^o. The best value for QW width to achieve the lesser threshold current density J_{th}=481.5 A/cm^2 when L_z =100A^o [65].

In 2015 HADJAJ Fatima, et al studied the characteristics electric of GaAs/Al$_{0.32}$Ga$_{0.68}$As quantum well laser diodes emitting at 0.8μm. Indicate results to the best output performance and lower threshold current could be obtained for a single quantum well and losses are reduced, we note also a gradual and nonlinear decrease in output optical power with the increase of temperature. Simulation electric characteristics of quantum well laser diodes helps understanding their behavior and provides an insight comprehension of the influence of technological parameters such as number of wells, cavity length and effect of temperature on their performance [66].

In 2016 MAJED KHODR studied the of internal quantum efficiency on PbSe / Pb$_{0.934}$Sr$_{0.066}$ MQW structure. The modal gain and threshold current density of this structure were calculated. The threshold current density and threshold current values increased by nearly 10 times when inclusion of theoretical internal quantum efficiency with no effects on the modal gain values [67].

1.11 Aim of the work

The present work aims at investigation the effect of structure parameters of multi quantum well laser ($Al_{0.01}Ga_{0.99}N/GaN$), such as wells number and barrier width, on the optical confinement factor, as well as the effect on the threshold current density and threshold current such as well width, average thickness, cavity length, mirror loss, threshold gain.

CHAPTER TWO

THEORETICAL CONCEPTS

2.1 Introduction

This chapter presents the necessary formulations for theoretical calculations of the significant parameters which are used in this work. Such as Schrodinger wave equation, Resonator modes, recombination carrier lifetime, Quasi Fermi level, optical transitions, optical confinement factor, optical gain in semiconductor laser, threshold current density and threshold current.

2.2 The Schrodinger Wave Equation

Electron diffraction in crystals can be described as indicating the nature of a wave of particles by the wave equation. The differential equation that describes the special dependence of the wave amplitude of a vibrating system can be written [68]

$$\nabla^2\Psi + (\frac{2\pi}{\lambda})^2\Psi = 0 \qquad (2\text{-}1)$$

Where

$$\nabla^2\Psi = \frac{\partial^2\Psi}{\partial x^2} + \frac{\partial^2\Psi}{\partial y^2} + \frac{\partial^2\Psi}{\partial z^2} \qquad (2\text{-}2)$$

By de Broglie formula for matter waves (i, e., $p = \frac{h}{\lambda}$ or $\lambda = \frac{h}{m\,v}$) where m is the electron mass, v is the wave velocity, h is the Planck constant and λ is the wavelength. The wave equation can be written as

$$\nabla^2\Psi + (\frac{2\pi\,m\,v}{h})^2\Psi = 0 \qquad (2\text{-}3)$$

This equation can be modulate by substituting the kinetic energy $(\frac{mv^2}{2})$ by the total energy E_t and potential energy V; $\frac{mv^2}{2} = E - V$. Therefore the wave equation become as the following

$$\nabla^2\Psi + \frac{2m}{\hbar^2}(E - V)\Psi = 0 \qquad (2\text{-}4)$$

This equation describes the properties of the electron wave, known as simply the Schrodinger equation or the time independent Schrodinger wave equation. That is a time independent equation suggests that the properties of the neighboring atomic to the electron do not differ with time [68]. The Schrodinger time-dependent equation should be used, if there is a time-varying periodic potential [68, 36].

$$\frac{-\hbar^2}{2m}\nabla^2\Psi + V\Psi = i\hbar\frac{\partial\Psi}{\partial t} \tag{2-5}$$

The Schrodinger equation for free electron is various from this equation for Bound electron in an infinitely deep potential well as the following.

2.2.1 Free Electrons

For free electrons and the spreading in the x direction with no potential barrier confining the electron wave propagation (i.e. V=0), eq. (2-4) become as the following [68]

$$\frac{d^2\Psi}{dx^2} + \frac{2m}{\hbar^2}E\Psi = 0 \tag{2-6}$$

The solution of this equation can be written as

$$\Psi(x) = A\exp(ikx) + B\exp(-ikx) \tag{2-7}$$

Where A and B constants, $k = (\frac{2m_eE}{\hbar^2})^{\frac{1}{2}}$. The first term in eq. (2-7) corresponds to a wave moving in the positive x direction while the second term corresponds to a wave moving in the negative x direction. From the above equation for k it follows that

$$E = \frac{\hbar^2k^2}{2m_e} \tag{2-8}$$

Shows that in the absence of boundary conditions, all values of energy are allowed for free electrons. Since $E = \frac{p^2}{2m_e}$, the momentum $p = \hbar k$, also $p = \frac{h}{\lambda} = \frac{2\pi\hbar}{\lambda}$, and thus $k = \frac{2\pi}{\lambda}$, where k is the wave vector of the electron [68]. Figure (2-1) for free electron, shows the relationship between momentum and energy, i. e., E (k) [68, 36].
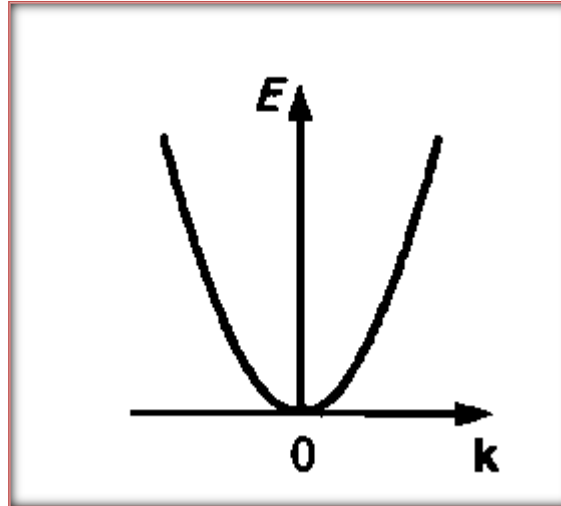
Figure (2-1): The relationship between energy E and wave vector k [68, 36].

2.2.2 Bound Electron in an Infinitely Deep Potential Well

Figure (2-2) show that electrons bound between two infinitely high potential barriers (but free to move inside the well), the potential energy inside the well V=0, the Schrodinger equation can be written for this one dimensional box as follows [68]

$$\frac{d^2\Psi}{dx^2} + \frac{2m}{\hbar^2}E\Psi = 0 \qquad (2\text{-}9)$$

The general solution to this differential equation can be expressed as follows

$$\Psi(x) = A\sin kx + B\cos kx \qquad (2\text{-}10)$$

Where

$$k = (\frac{2m_e E}{\hbar^2})^{\frac{1}{2}} \qquad (2\text{-}11)$$

In this specific case A and B can be determined through considering: Ψ (0) =0 and Ψ (L) =0. Thus, for x=0, Ψ (0) =B, and Ψ (x=L) can be written as

$$\Psi\ (L) = A \sin kL = 0 \tag{2-12}$$

Which is satisfied only if kL is an integral multiple of π, if kL = n π, where n = 0, 1, 2, 3, 4, … Since $E = \dfrac{\hbar^2 k^2}{2m_e}$

$$E_n = \frac{\hbar^2 n^2 \pi^2}{2m_e L^2} \tag{2-13}$$
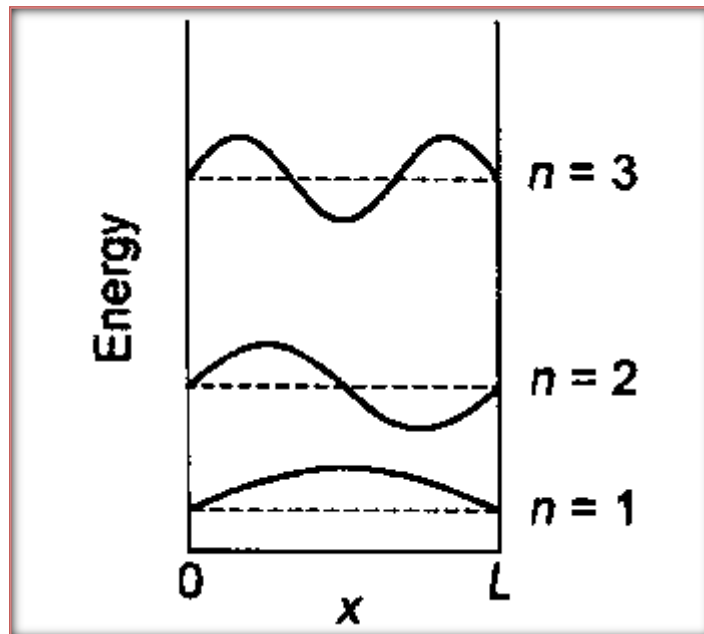
Figure (2-2): The diagram of the ground state and two excited state energy levels and associated wave function for an infinity deep square potential well [68].

2.3 Resonator Modes

2.3.1 Longitudinal Modes

A longitudinal mode of a resonator cavity is a particular standing wave pattern formed by waves confined in the cavity. After many reflections from the surface of the reflective for the cavities, the longitudinal modes correspond to the wavelengths of the wave which are reinforced by constructive interference. By the destructive interference all the other

wavelengths are suppressed. A beam is a structural component by the resisting bending to be the able of withstanding load primarily. The bending moment is defined as the bending force induced into the material of the beam as a result of the own weight, external loads, span and external reactions to these loads [69].

2.3.2 Transverse Modes

A transverse mode of a ray of the electromagnetic radiation is a special electromagnetic field mode of radiation measured in a vertical plane to the propagation (i.e, transverse) direction of the ray. Transverse modes occur in the radio waves and microwaves, also happen in lasers optical resonator and the light waves in the optical fiber. Transverse modes occur due to the boundary conditions imposed on the wave of the waveguide. For this reason the modes buoyed by a waveguide is quantized. It can be found the allowed modes through solving Maxwell's equations for the boundary conditions of a given waveguide [70].

There are two types of transverse mode as the following.

2.3.2.1 Transverse Magnetic (TM) Modes

In the TM modes there is no magnetic field in the direction of propagation. There is only an electric field along the direction of propagation and for this reason is sometimes called E modes [70].

2.3.2.2 Transverse Electric (TE) Modes

In the TE modes there is no electric field in the direction of propagation. There is only a magnetic field along the direction of propagation and for this reason is sometimes called H modes [70].

2.4 Recombination Carrier Lifetime

The carrier recombination is the reverse process for generation process [71].The generation defined as the movement of an electron from the valence band to the conduction band. This leads to the creation of the electron hole pair [72]. Recombination is that the process in which the electrons return from conduction band to valence band, which emit the energy in form light or photons. The lifetime of the minority carrier controls the rate of recombination. Recombination process is classified into two type radiative recombination and non radiative recombination [71].

2.4.1 Radiative Recombination

The radiative recombination occurs when electron in the conduction band recombines with hole in the valence band emitting a photon as shown in figure (2-3a). Radiative recombination process can be spontaneous emission or stimulated emission.
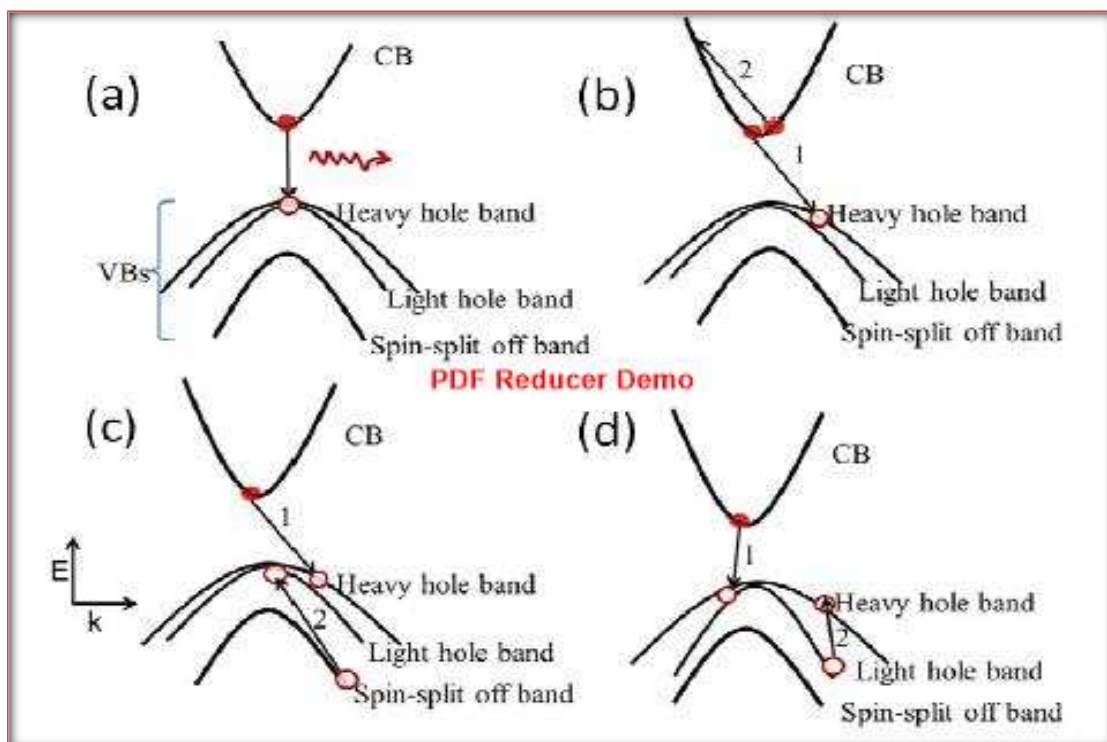
Figure (2-3): Radiative recombination and nonradiative Auger recombination [73].

The radiative recombination rate due to spontaneous emission can be expressed by the following equation

$$R_r = B_{rad} N^2 \qquad (2\text{-}14)$$

Where N is the carrier concentration, B_{rad} is the radiative recombination coefficient [73], can be written as [74]

$$B_{rad} = \frac{e^2 \, w \, n_r \, E_g \, |M_{ave}|^2}{\varepsilon_o \, C^3 m_o^2 \, k_b \, T \, m_h^*(1+r)} \qquad (2\text{-}15)$$

Where e is the electron charge, w is the well width, E_g is the energy band gap, ε_o is the permittivity in vacuum, C is the light velocity, m_o is the free electron mass, k_b is the Boltzmann constant, $r = \frac{m_e^*}{m_h^*}$, n_r is the refractive index, $|M_{ave}|^2$ is the average of the squared of the momentum matrix element can be written as [75, 76, 77]

$$|M_{ave}|^2 = \frac{(2M_{TE} + M_{TM})}{3} \qquad (2\text{-}16)$$

Where M_{TE} is an average of the squared momentum matrix element for the TE mode when quantized energy of the nth subband equal E_n can be written as [56]

$$M_{TE} = \langle M^2 \rangle_{hh,TE} + \langle M^2 \rangle_{lh,TE} \qquad (2\text{-}17)$$

Where $\langle M^2 \rangle_{hh,TE}$ and $\langle M^2 \rangle_{lh,TE}$ are the squared momentum matrix element of the electron-heavy hole and electron-light hole interactions respectively for the TE mode as the following [9].

$$\langle M^2 \rangle_{hh,TE} = \frac{3M^2}{2} \qquad (2\text{-}18)$$

$$\langle M^2 \rangle_{lh,TE} = \frac{M^2}{2} \qquad (2\text{-}19)$$

And M_{TM} is an average of the squared momentum matrix element for the TM mode when quantized energy of the nth sub band equal E_n can be written as [56].

$$M_{TM} = \langle M^2 \rangle_{hh,TM} + \langle M^2 \rangle_{lh,TM} \qquad (2\text{-}20)$$

Where $\langle M^2 \rangle_{hh,TM}$ and $\langle M^2 \rangle_{lh,TM}$ are the squared momentum matrix element of the electron - heavy hole and electron - light hole interactions respectively for the TM mode as the following [9].

$$\langle M^2 \rangle_{hh,TM} = 0 \qquad (2\text{-}21)$$

$$\langle M^2 \rangle_{lh,TM} = 2M^2 \qquad (2\text{-}22)$$

Where M is the momentum matrix element can be written by the following express [9]

$$M = \frac{m_o}{\sqrt{3}} \left(\frac{E_g(E_g + \Delta_o \ )}{2m_e^*(E_g + \frac{2}{3}\Delta_o)} \right)^{\frac{1}{2}} \qquad (2\text{-}23)$$

Where is Δ_o is the split off energy.

2.4.2 Non Radiative Recombination

Non radiative recombination process is the most important in understanding of the semiconductor physics in optoelectronic devices for example light emitting diodes and solar cells [78]. Non radiative recombination happens when the carriers in the (CB) and (VB) recombine non- radiatively, this means that will not light emit from this process. This will increases the current need to achieve lasing [10]. Non radiative recombination can decrease device efficiency by reducing the collection of photo-generated carriers and suppressing luminescence or carrier lifetimes [78]. Non radiative recombination process includes defects recombination, Auger recombination and leakage current recombination.

2.4.2.1 Defects Recombination:

Defects rise from the aberrations in the crystalline structure of the semiconductor material. They are normally formed through epitaxial growth; an atomic place can be replaced by an impurity, or change leaving place by vacant place which would ordinarily be employed, or it is sometimes occupying by an atom which is supposed to empty place. These defects states (electrons and holes) can be recombining non-radiatively within a diffusion length. The defect rate related to recombination by the following expression [73]

$$R_D = A_D N \qquad\qquad\qquad (2\text{-}24)$$

A_D is the monomolecular recombination coefficient.

2.4.2.2 Auger Recombination:

The recombination energy of electron and hole is added to another electron (hole) which is transited to a higher energy level in the (CB) and lesser energy level in the (VB). To realize thermal equilibrium, the carrier which is in excited state relaxes by emits a phonon through lattice vibration.

Auger recombination is delicate to band gap. It increases as the semiconductor band gap decreases and then it products major problem in the mid infrared devices. This is due to the decrease in the band gap energy, the effective mass of carriers and the activation energy decreases lead to increasing the probability of Auger process. The Auger process shows in Figure (2-3)

The momentum in a band to band Auger process is preserved in an electron-hole transition and is not presented phonons. It is categorized into three based dependent on the bands in which the Auger carriers excited to and or are reside. Figure (2-3b) shown conduction-hole conduction-conduction (CHCC) Auger process. In this process the electron transits from conduction

band to valence band without emitting a photon; instead of the energy excites another electron in conduction band to a higher energy state. Later the excited electron misses the additional energy by optical phonons and the system reaches to the thermal equilibrium. Another form of direct band to band Auger is the conduction-heavy hole- spin-split off band is excited to the heavy hole Auger recombination (CHSH) shown in figure (2-3c). In the conduction-hole-light-heavy-hole (CHLH) Auger process shown in figure (2-3d), an electron in the spin- split off band is excited to the heavy-hole band, if the electron-hole process leads to a transition from a light-hole band to the heavy-hole [73].

The Auger recombination rate can be written as the following [79]

$$R_{Aug} = \left(C_p + C_n\right)n^3 = C_{Aug}N^3 \qquad (2\text{-}25)$$

Where C_p, C_n are the Auger coefficient electron and hole respectively and C_{Aug} is the Auger recombination coefficient can be written as [73]

$$C_{Aug} = \frac{1}{\zeta_A N^2} = C_o \exp\left(\frac{-E_a}{k_b T}\right) \qquad (2\text{-}26)$$

Where ζ_A is the Auger carrier lifetime.

E_a and C_o are the activation energy and coefficient in the (CHCC) Auger process can be written [74]

$$E_a = \frac{m_e E_g}{m_e^* + m_{hh}} \qquad (2\text{-}27)$$

$$Co = \frac{4\pi e^4 m_e (m_{hh} + m_e^*)|M_{ee}|^2}{\hbar \varepsilon^2 (2m_{hh} + m_e^*)^2 k_B T} \qquad (2\text{-}28)$$

Where m_{hh} the heavy hole mass, ε is the dielectric constant, $|M_{ee}|^2$ is the matrix element of the electron-electron interaction is given by

$$|M_{ee}|^2 = (\frac{\hbar^2}{2m_o})^2 \frac{m_o E_p}{3\, m_e^* E_g^3} \qquad (2\text{-}29)$$

Where E_p is the energy equivalent of the momentum matrix element.

Thus the total recombination rate can be express as [80]

$$R_{total} = R_r + R_D + R_{Aug} \qquad (2\text{-}30)$$

The recombination lifetime can be expressed in the following equation [80]

$$\frac{1}{\tau_{rec}} = \frac{1}{\tau_r} + \frac{1}{\tau_D} + \frac{1}{\tau_{Aug}} \qquad (2\text{-}31)$$

2.5 Quasi Fermi Level

The allowed energy levels for electrons and holes in a semiconductor crystal represent the band structure. The probability of presence the electrons in allowed energies expressions by Fermi Dirac function as the following [48]

$$f(E) = \frac{1}{1+\exp(\frac{E-E_f}{k_b T})} \qquad (2\text{-}32)$$

Where $f(E)$ is the probability of finding an electron at energy E, E_f is the Fermi energy. In thermal equilibrium, Fermi level determines the occupation probabilities. In non- equilibrium, such as when a material is pumped to achieve lasing , separate Fermi levels , termed quasi Fermi levels , are defined for the conduction band and valence band. The occupation probability may then be determined through positions of the two quasi Fermi levels, defined to account for carrier concentrations in the two bands separately.

Define the energies of the electrons and holes are separately to reflect the non-equilibrium case. For the valence band, E_h is the hole energy, E_v below the valence band energy, the corresponding quasi Fermi level is given by E_{fv}. In the conduction band, E_e is the electron energy, E_c above the conduction

band energy and the corresponding quasi Fermi level is E_{fc}, as shown in figure (2-4).
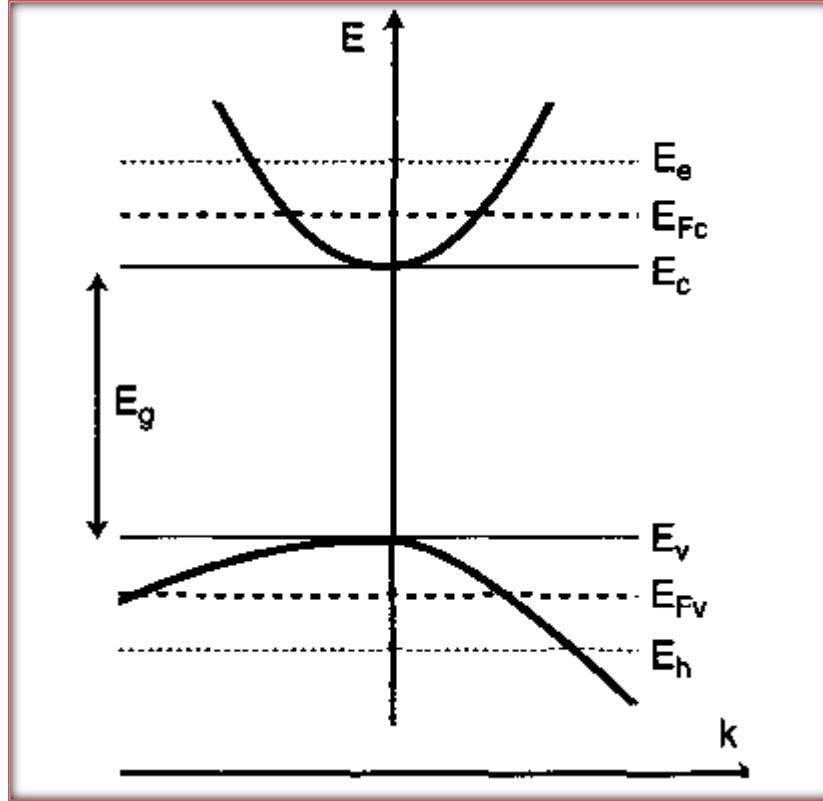
Figure (2-4): Definition of the quasi Fermi levels and electron and hole energies [48]

These descriptions for the quasi Fermi levels, the occupation probability for electrons in the conduction band f_c (E), and holes in the valence band f_v (E), can be expressed as a function of electron and hole energies by [9, 48]

$$f_c(E) = \text{f (E)} = \frac{1}{1+\exp\frac{(E_e - E_{fc})}{k_b T}} \tag{2-33}$$

$$f_v(E) = \text{1-f (E)} = \frac{1}{1+\exp\frac{(E_{fv} - E_h)}{k_b T}} \tag{2-34}$$

$$E_{fc} = E_c + k_b T \ln(\frac{N}{N_c}) \tag{2-35}$$

$$E_{fv} = E_v - k_b T \ln(\frac{P}{N_v}) \tag{2-36}$$

Where N and P the electrons and holes concentration, respectively, N_c and N_v are the effective density of states for electrons and holes, respectively can be written [48].

$$N = N_c \exp \frac{(E_{fc} - E_c)}{k_b\, T} \qquad\qquad (2\text{-}37)$$

$$P = N_v \exp \frac{(E_v - E_{fv})}{k_b\, T} \qquad\qquad (2\text{-}38)$$

$$N_c = 2(\frac{2\pi\, m_e^*\, k_b\, T}{h^2})^{\frac{3}{2}} \qquad\qquad (2\text{-}39)$$

$$N_v = 2(\frac{2\pi\, m_h^*\, k_b\, T}{h^2})^{\frac{3}{2}} \qquad\qquad (2\text{-}40)$$

The transparency carrier density can be determined by the following equation [9, 81]

$$N_{tr} = \sqrt{N_c - N_v} = [2(\frac{k_b\, T}{2\, \hbar^2})^{\frac{3}{2}} (m_e^* m_h^*)^{\frac{3}{4}}] \qquad\qquad (2\text{-}41)$$

In thermal equilibrium, the quasi Fermi levels are equal to each other, therefore equal to the Fermi level, or $E_{fc} = E_{fv} = E_f$ [9, 48].

2.6 Optical Transitions

Optical absorption and emission happen through the interaction of optical radiation with electrons in a material system that defines the energy level of the electrons. Depending on the characteristics of a particular material, electrons that interact with optical radiation can be either those bound to individual atoms or those exist in the energy band structures of a material such as semiconductor. The absorption or emission of a photon by electrons is related with a resonant transition of the electron between a lesser energy level 1 of energy E_1 and higher energy level 2 of energy E_2. Band to band transition in a semiconductor occur through transition an electron between valence and conduction bands, there are two types band to band transition is direct and indirect transition. A direct transition occurs when an electron makes an

upward or downward transition without the contribution of a phonon. Indirect transition when an electron makes it has to absorb or emit a phonon, thus exchanging energy and momentum with crystal lattice, and so to complete the transition [26]. Optical transition consists of two kinds' interband transition and intraband transition. Interband transitions occur between the conduction band and valence band, and include two types electrons and holes. Intraband transitions occur inside either conduction band or the valence band, and involve only one kind of carrier [82]. Figure (2-5) show different optical transitions in semiconductors. Figure (2-5a) display interband transitions and intraband transitions in bulk semiconductor structure happen between bands and inside a band, respectively. And also show that the transition matrix element for interband (band to band) stimulated absorption is non-zero. The transition matrix element for intraband stimulated absorption is zero. Figure (2-5b) show interband transitions in quantum well structures happen between quantized states in the conduction band well and quantized states in the valence band well. Let us allocate these transitions an energy E_{mn}, where m is the m_{th} quantized state in the conduction band well and n is the n$_{th}$ quantized state in the valence band well. For example, the E00 transition happens among the two ground states of the wells. Show that transitions allowed is E$_{00}$, E$_{02}$, E$_{20}$... and that E$_{01}$, E$_{10}$, E$_{12}$... are disallowed transitions. The allowed interband transitions are characterized by Δ=m-n=0, 2, 4 ...,fig.(2-5c) shows that intraband transitions in quantum well structures happen between quantized states in the same well. Such intraband transitions typically occur in the far infrared. Thermally sensitive cameras are based on this principle. Let us allocate these transitions energy E_{mn}, where m is the m_{th} quantized state in the well and n is the nth quantized state in the well. For example, the E$_{10}$ transition happens between the first excited state and the ground state of the well. The transitions allowed is E$_{01}$, E$_{03}$, E$_{12}$ ... and that E$_{02}$, E$_{04}$, E$_{24}$ ... are

disallowed transitions. Show that allowed intraband transitions are characterized by Δ=m-n=1, 3, 5 … [83]
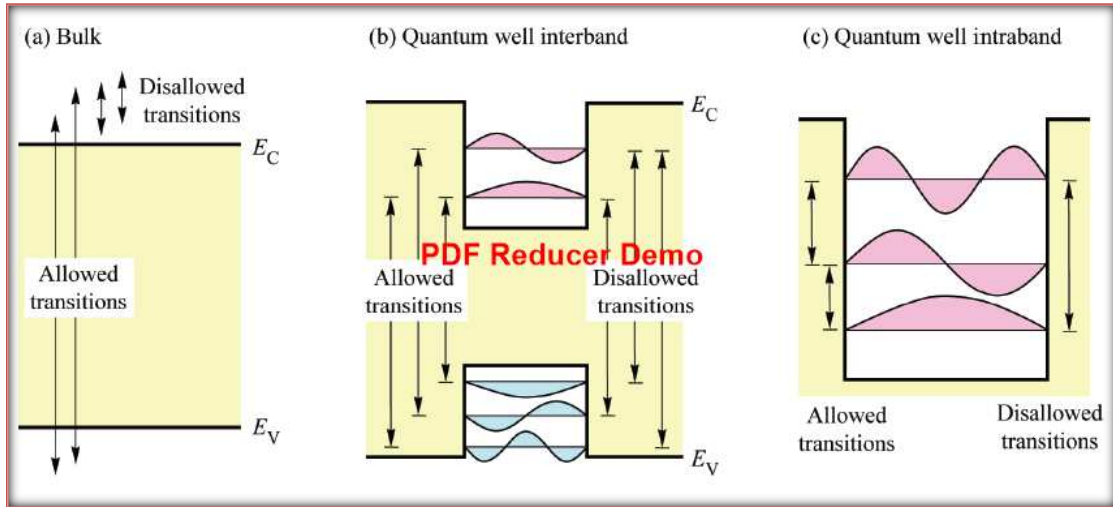
Figure (2-5): Allowed and disallowed interband and intraband transitions in bulk and quantum well semiconductor [83].

2.7 Optical Confinement Factor

The optical confinement factor is necessary for the accurate modeling of the semiconductor lasers. The optical confinement factor is defined as the fraction of the energy of the specific waveguide mode confined to the active region [84].Also defined as the fraction of the squared electric field confined to the active region [85]. Due to the light distributes as shown in figure (2-6), the optical confinement factor for the film, which is shown as a shaded area is given by [9]

$$\Gamma = \frac{\int_0^h |E_x^2|\, dx}{\int_{-\infty}^{\infty} |E_x^2|\, dx} \tag{2-42}$$
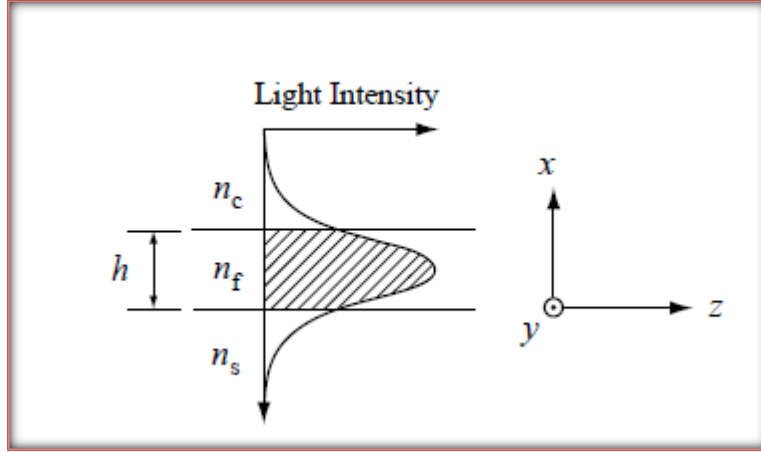
Figure (2-6): The distribution of light intensity [9].

Expression of the optical confinement factor in a SQW is given by the following equation [84, 86]

$$\Gamma^{SQW} = \frac{D^2}{D^2+2} \qquad (2\text{-}43)$$

Where D is the normalized thickness of the active region is given by

$$D= 2\pi \left(\frac{w}{\lambda}\right) \sqrt{(n_{r,w}^2 - n_{r,c}^2)} \qquad (2\text{-}44)$$

Where w is the well width, $n_{r,w}$ is the refractive index of the active region layer, $n_{r,c}$ the refractive index of the cladding layer.

The optical confinement factor for (MQW) can be written as [86]

$$\Gamma^{MQW} = \Gamma^{SQW} \frac{N_w w}{d} \qquad (2\text{-}45)$$

Where d is the average thickness of active region, and can be written as:

$$d = (N_w\, w + N_b\, b) \qquad (2\text{-}46)$$

Where N_w the number of wells, N_b is the number of barriers denoted by $(N_w\text{-}1)$, b is the barrier thickness.

$$D' = 2\pi\left(\frac{d}{\lambda}\right)\sqrt{n_{\bar{x}}^2 - n_{r,c}^2} \qquad (2\text{-}47)$$

Where $n_{\bar{x}}$ is the average refractive index, can be written

$$n_\gamma = \frac{N_w w\, n_{r,w} + N_b b\, n_{r,b}}{d}$$
(2-48)

Where $n_{r,b}$ is the refractive index of the barrier material , in the optical confinement factor for MQW using $D^{'}$ instead D in the equation (2-43) [86].The optical confinement factor is important to design the optical losses or the optical gains in the optical waveguides [9].

2.8 Optical Gain in Semiconductor Laser

The optical gain is the growth ratio of light intensity (photon density) per unit length of light spread. The optical gain is proportional with possibility that a given photon lead an electron transition of the high energy level j to the less energy level i. The transition energy E_{ij} = E_j- E_i must be equal to the photon energy hυ. The quantum mechanical calculation of this possibility for semiconductor has been described in several publications. To provide a more intuitive understanding, we skip most of the quantum mechanics here and evaluate the simple gain function

$$g_{ij}(h\upsilon) = \left(\frac{e^2\, h}{2\, m_0^2 \varepsilon_o\, n_r\, C}\right)\left(\frac{1}{h\,\upsilon}\right)\left|M_o(E_{ij})\right|^2 D_r(E_{ij})(f_j - f_i)$$
(2-49)

For hυ = E_{ij}.where $|M_o|^2$is the transition matrix element, $D_r(E)$ is the density of allowed transition between two bands [87].

The gain of the system must at least be equal to the losses in this system; this gain is called a threshold gain. The beam intensity as it leaves the medium will be [13]

$$I = I_o e^{(g_o - \alpha_i)L}$$
(2-50)

This beam intensity is reflected from mirror 1, reflection becomes as the following

$$I = I_o \, R_1 e^{(g_o - \alpha_i)L} \tag{2-51}$$

Another transition through the medium by a reflection from mirror 2, the beam intensity after one trip through the resonator is written as

$$I = I_o G_g = I_o R_1 R_2 e^{2(g_o - \alpha_i)L} \tag{2-52}$$

Where I_o is initial beam intensity as it leaves mirror 2, R_1, R_2 is the reflection or reflectivity coefficient of the two mirrors, α_i is the internal loss, g_o is the gain coefficient and G_g is the round-trip power gain oscillation.

When $I \geq I_o$

$$G_g = R_1 R_2 e^{2(g_o - \alpha_i)L} \geq 1 \tag{2-53}$$

This condition necessary to achieve oscillation in the resonator, and the threshold for oscillation is given by the minimum bound. The steady-state condition is $I = I_o$.

The threshold gain is given by [8, 13].

$$g_{th} = \alpha_i + \alpha_m \tag{2-54}$$

Where α_i is the internal loss and α_m is the mirror loss, and can be written

$$\alpha_m = \frac{1}{2L} \ln\left(\frac{1}{R_1 R_2}\right) \tag{2-55}$$

The threshold gain in MQW can be written [81]

$$g_{th} = \frac{\alpha_i + \alpha_m}{\Gamma^{MQw}} \tag{2-56}$$

2.9 Threshold Current Density

The symbol of the threshold current density is (J_{th}). Threshold current density is a direct indicator in determining the quality of semiconductor materials that are fabricated device [88].

The threshold current density is given by [89, 90]

$$J_{th} = ed(A_D N_{th} + B_{rad} N_{th}^2 + C_{Aug} N_{th}^3)$$ (2-57)

Where N_{th} is the threshold carrier density and can be expressed as [81].

$$N_{th} = N_{tr} \, exp^{(\frac{\alpha_i + \alpha_m}{\Gamma MQW \, g_o})}$$ (2-58)

Where g_o is the gain coefficient.

2.10 Threshold Current

The threshold current (I_{th}) is the basic and most important parameter from the laser diodes. Under the threshold, the light emitted in the active layer spreads along the layer because the refractive index of the active layer is higher than that of the cladding layers [5].When applied forward current is less than threshold current, the laser diode works like (LED) .where the density of carriers in the active layer is not high enough for population inversion, the spontaneous emission dominates and creating a small quantity of incoherent light as shown in the figure (2-7).
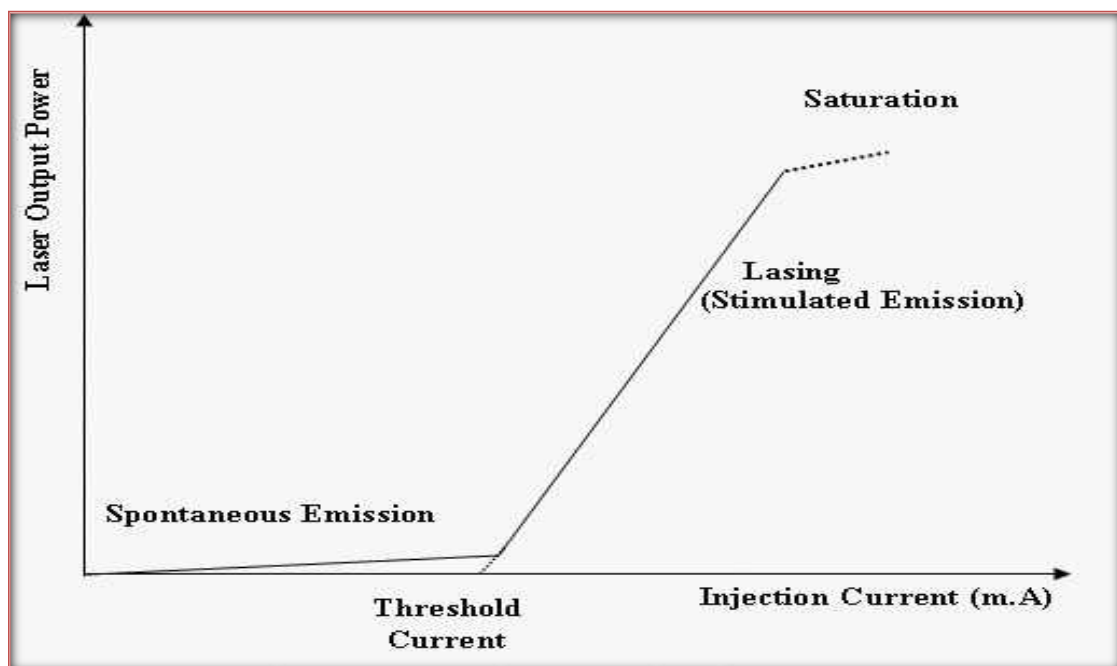
Figure (2-7): The variation output power with current curve [91].

by increasing the bias, population inversion happens, stimulated emission becomes predominant and cavity losses are requite at a certain bias current, at this point, the current is named threshold current. The injection current above the threshold produces the sudden start of lasing action and coherent light is emitted from the laser diode. The threshold current of laser evaluated by reasoning the linear part of the characteristic to zero output power [91].

Threshold current can be calculated by the following equation [67, 86]

$$I_{th} = J_{th} \text{ Area} = J_{th} \text{ L W} \qquad\qquad (2\text{-}59)$$

Where J_{th} is the threshold current density, L and W are the length and width of cavity laser.

Threshold current is dependent on the quality of the semiconductor material and the general design of the waveguide structure, the size and area of the laser device [88], also temperature depends can be described by [92]

$$I_{th}(T_2) = I_{th}(T_1) \, exp^{(\frac{T2-T1}{To})} \qquad\qquad (2\text{-}60)$$

Where T_2 and T_1 is the different package temperature, T_0 is the temperature constant of the threshold current.

CHAPTER THREE

RESULTS AND DISCUSSION

3.1 Introduction

This chapter contains the results that are acquired through the application of expression which are described in chapter two. In this chapter we determined the x value of $Al_xGa_{1-x}N$/GaN multi-quantum well structure. Thus calculated the MQW structure parameters such as barrier width (b), number of well (N_w), and number of barrier (N_b). From the effecting of these parameters on optical confinement factor, determined those values according to the best value of optical confinement factor. Then study the laser diode parameters such as well width (w), cavity length (L), reflectivity of cavity mirror (R_1, R_2), Cavity Width (W), Average thickness of active region (d), optical confinement factor (Γ), mirror losses and threshold gain which are effect on threshold current density and threshold current to determine the optimum value of threshold current. All these parameters are calculated for multiple quantum well of $Al_{0.01}Ga_{0.99}N$/GaN heterostructure laser system. This structure emitted wavelength (λ=352 nm) in ultraviolet (UV) radiation range. Ultraviolet (UV) radiation is a part of the electromagnetic spectrum between the X-rays and visible light. The UV is classified into Vacuum UV (40-190 nm), Far UV (190-220 nm), short (UVC) (220-290 nm), medium UV (UVB) (290-320 nm) and long UV (UVA) (320-400 nm) [93, 94]. From these ranges, the emitting wavelength for AlGaN/GaN multi-quantum well structure is in UVA range. The wavelength which used has several applications such as forensic analysis, protein analysis, drug detection, DNA sequencing, optical sensors, various instrumentation, medical imaging of cells, curing of polymers, in the treatment of psoriasis, eczema and vitiligo [93].

3.2 Scope of the Work

The material used in this study is AlGaN/GaN. We used Matlab version 8.2.0.701 (2013) to draw figures and calculations. Figure (3-1) is a block

diagram of the laser diode parameters of the work scope. The constants are used in calculation of this chapter in the tables (3-1), (3-2) and (3-3).

Table (3-1): List of constant

Symbol	Constant	Values	Unit
Electron charge	e	$1.6*10^{-19}$	C
Plank's constant	h	$4.140*10^{-15}$	eV.s
Plank's constant divided by 2π	$\hbar$	$0.659*10^{-15}$	eV.s
Free electron mass	m_o	$9.1*10^{-31}$	Kg
permittivity in vacuum	ε_o	$8.85*10^{-12}$	$C^2/N.m^2$
Boltzmann's constant	k_b	$8.6250*10^{-5}$	eV/K
Temperature	T	300	K

Table (3-2): Properties of GaN

Symbol	Constant	Values	Unit	Ref. No
Electron effective mass	m_e^*	$0.2m_o$	Kg	52
Hole effective mass	m_h^*	$0.8\ m_o$	Kg	52
Heavy hole mass	m_{hh}	$1.4\ m_o$	Kg	52
Energy gap	E_g	3.43	eV	49, 51
Dielectric constant	ε	$8.9\ \varepsilon_o$	$C^2/N.m^2$	52
Refractive index	n_r	2.5067	Non	54
Gain coefficient	g_o	$1.5*10^5$	m^{-1}	95
Energy equivalent of the momentum matrix element	E_p	14	eV	51
Split off energy	Δ_o	$14*10^{-3}$	eV	51
Monomolecular recombination coefficient	A_D	$1*10^8$	s^{-1}	96
Internal loss	α_i	25	cm^{-1}	97
Reflectivity mirror 1	R_1	0.75	Non	Non
Reflectivity mirror 2	R_2	0.9	Non	Non

Table (3-3): Properties of AlN

Symbol	Constant	Values	Unit	Ref. No
Refractive index	n_r	1.99	Non	52 ,98

Laser Diode

Structure

Homojunction

Heterojunction

SH

DH

QW

SQW

MQW

Laser Diode Parameter

$$|M_{ave}|^2 = \frac{(2\,M_{TE} + M_{TM})}{3}$$

$$|M_{ee}|^2 = (\frac{\hbar^2}{2m_o})^2 \frac{m_o E_p}{3m_e^* E_g^3}$$

$$N_{tr} = 2(\frac{k_b T}{2\pi \hbar^2})^{\frac{3}{2}}(m_e^* m_h^*)^{\frac{3}{4}}$$

Optical confinement factor

$$B_{rad} = \frac{e^2 W n_r E_g |M_{ave}|^2}{c^3 \varepsilon_o m_o^2 E_g k_B T m_h^* (1+R)}$$

$$Co = \frac{4\pi e^4 m_e (m_{hh} + m_e)|M_{ee}|^2}{\hbar \varepsilon^2 (2m_{hh} + m_e)^2 k_B T}$$

$$d = N_w w + N_b b$$

$$n_\gamma = \frac{N_w w n_{r,w} + N_b b n_{r,b}}{d}$$

$$E_a = \frac{m_e^* E_g}{m_e^* + m_{hh}}$$

$$C_{Aug} = C_o \exp\left(\frac{-E_a}{k_b T}\right)$$

$$D^{'} = 2\pi(\frac{d}{\lambda})\sqrt{n_\gamma^2 + n_{r,c}^2}$$

$$\Gamma^{SQW} = \frac{D'^2}{D'^2 + 2}$$

$$\Gamma^{MQW} = \Gamma^{SQW} \frac{N_w w}{d}$$

$$\eta_{rad} = \frac{B_{rad} N_{th}}{A + B_{rad} N_{th} + C_{Aug} N_{th}^2}$$

$$N_{th} = N_{tr} e^{\frac{\alpha_i + \alpha_m}{g_o \Gamma^{MQW}}}$$

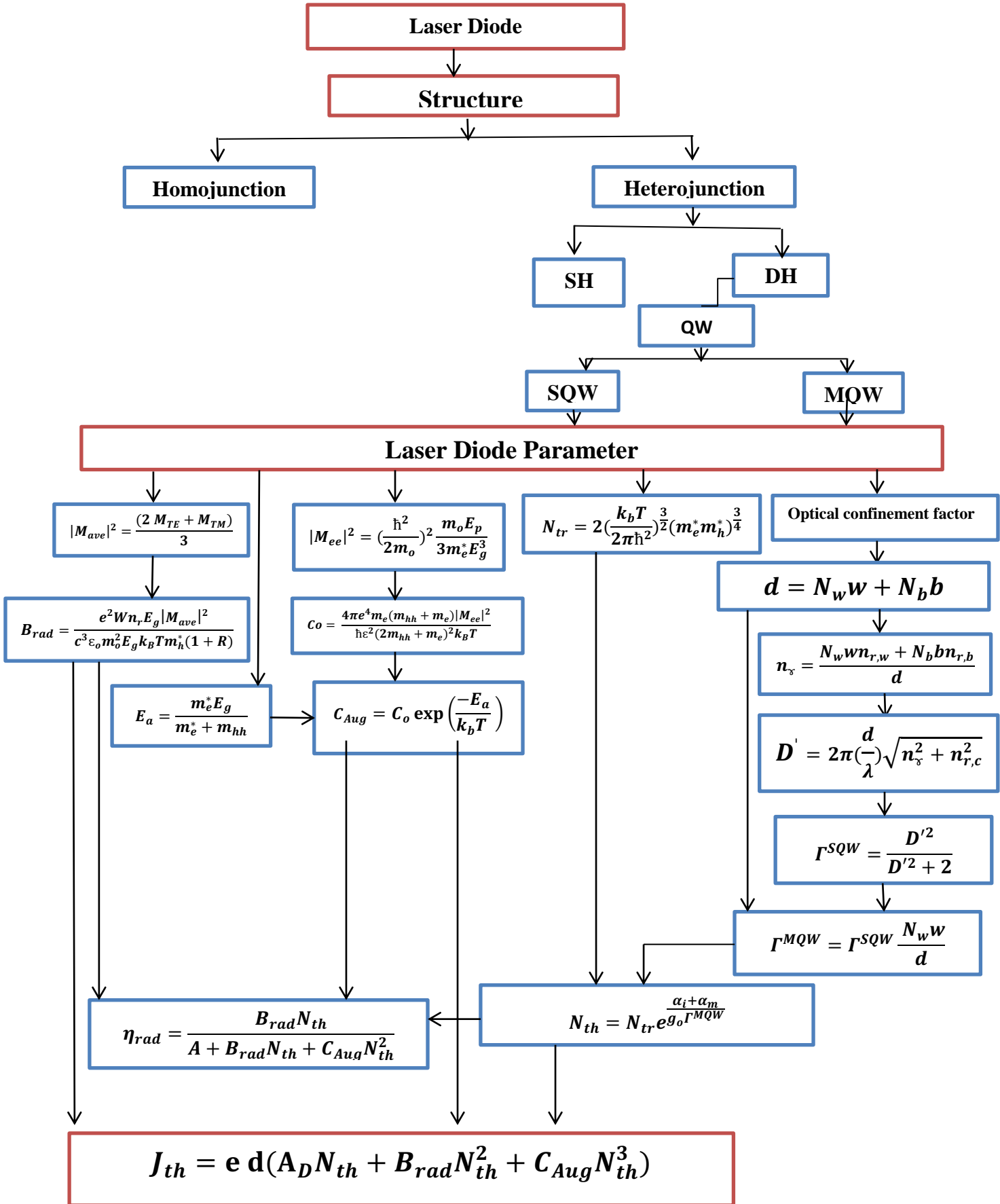$$J_{th} = e\,d(A_D N_{th} + B_{rad} N_{th}^2 + C_{Aug} N_{th}^3)$$

Figure (3-1): A Block diagram of the laser diode parameters of the work scope

The multiple quantum well laser system consists from wells and barriers. The material of the well layer is GaN and the cladding layer is AlN. The barrier layer material is choosing by checkup the values of mole fraction (x) for Al which gives higher value of optical confinement factor. This exam illustrates in table (3-4).

Table (3-4): Optical confinement factor versus the mole fraction x for different number of well.

N_w	$N_w=2$		$N_w=3$		$N_w=4$		$N_w=5$	
x_b	w(nm)	Γ	w(nm)	Γ	w(nm)	Γ	w(nm)	Γ
0.01	22.2	0.4107	12.2	0.3276	7	0.2413	4.3	0.1761
0.02	22	0.407	11.9	0.3203	6.9	0.238	4.2	0.1724
0.03	21.8	0.4032	11.8	0.3174	6.8	0.2346	4.2	0.1721
0.04	21.7	0.401	11.7	0.3146	6.8	0.2341	4.2	0.1718
0.05	21.5	0.3972	11.6	0.3117	6.8	0.2337	4.1	0.168
0.06	21.4	0.395	11.5	0.3088	6.8	0.2333	4.1	0.1677
0.07	21.2	0.3911	11.3	0.3036	6.7	0.2299	4.1	0.1674
0.08	21	0.3872	11.3	0.303	6.7	0.2294	4.1	0.1671
0.09	20.9	0.385	11.2	0.3001	6.7	0.2289	4.1	0.1668
0.1	20.8	0.3828	11.2	0.2996	6.7	0.2285	4.0	0.163
0.15	20.6	0.3768	11	0.2919	6.6	0.2232	4.0	0.1614
0.2	20	0.3637	10.9	0.2865	6.6	0.2207	4.0	0.1597
0.25	19.2	0.3466	10.8	0.2811	6.5	0.2152	3.9	0.1544
0.29	18.9	0.339	10.4	0.2688	6.4	0.2101	3.9	0.1529

It illustrates that the optical confinement factor (Γ) as a function of well width for different values of mole fraction (x) of Al in $Al_xGa_{1-x}N$ has been calculated by using eq. (2-45). This table shows that the higher value of Γ is 0.4107 at $x = 0.01$ and number of well is 2. Therefore the barrier layer is $Al_{0.01}Ga_{0.99}N$ material.

3.3 Parameters Affecting the Optical Confinement Factor

The best value of optical confinement factor (Γ) is used to determine the values of number of well (N_w), number of barrier (N_b) and barrier width (b) for our structure which is $Al_{0.01}Ga_{0.99}N$ /GaN multiple quantum well. These parameters determined by the relationship between the optical confinement factor and well width.

3.3.1 Well width (w), Well Number (N_w) and Barrier Width (b)

The optical confinement factor for $Al_{0.01}Ga_{0.99}N$ /GaN multiple quantum well systems was calculated from eq. (2-45). Figure (3-2) shows that the optical confinement factor (Γ) versus well width (w) for different barrier widths (2, 4, 8, 12, 20) nm. In this figure there are four cases of well numbers (N_w) (2, 3, 4, 5). It shows that the optical confinement factor (Γ) is increasing with increases well width (w) for each value of the barrier widths for multiple quantum well (MQW). It is clear from this figure that there exists a value of well width intersected all the curves of different barrier width at exact value of optical confinement factor. However, for w lower than this value, it appears that the varying rate of Γ with rising barrier width can be ignored, whereas higher than this value the varying rate of optical confinement factor for b of 2 nm is more than of other barriers.

Figure (3-2a) illustrates that well number is two, well width is 22.2 nm and the optical confinement factor is 0.4107, while in figure (3-2b), well number is three, well width is 12.2 nm and the optical confinement factor is 0.3276, in

figure (3-2c), well number is four, the well width is 7 nm and the optical confinement factor is 0.2413, in figure (3-2d), well number is five, the well width is 4.3nm and the optical confinement factor is 0.1761. We note that the highest value for the optical confinement factor is $\Gamma = 0.4107$ when a well number ($N_w = 2$) and the barrier width b=2 nm. Therefore, we choose number of well ($N_w = 2$) and barrier width b = 2 nm as optimization values for our structure ($Al_{0.01}Ga_{0.99}N/GaN$).

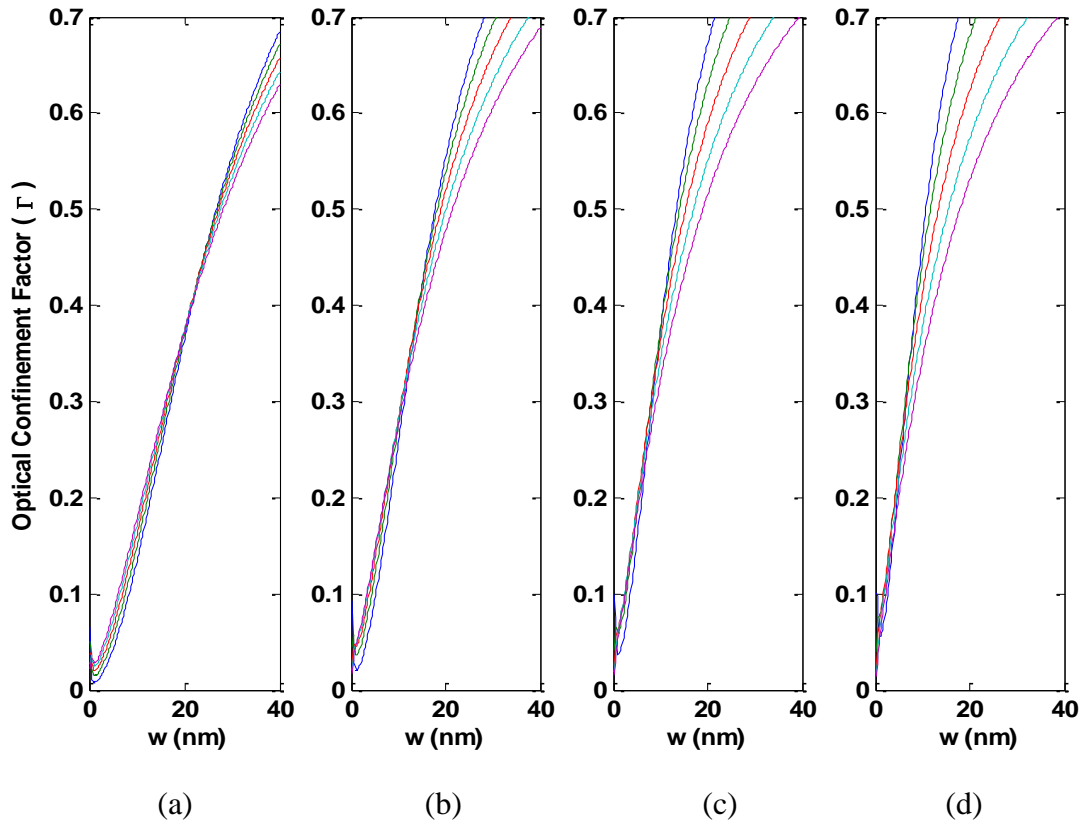<div align="center">(a)   (b)   (c)   (d)</div>

Figure (3-2): Optical confinement factor versus width of well for the different barrier width (a) $N_w = 2$ (b) $N_w = 3$ (c) $N_w = 4$ (d) $N_w = 5$ where ___ b=2nm, ___b=4nm, ___b=8nm, ___b=12nm, ___b=20nm.

3.4 Parameters Affecting on the Threshold Current Density and Threshold Current
3.4.1 Well Width (w)

The threshold current density (J_{th}) as a function of the well width (w) for different cavity length L = (0.5, 0.75, 1, 2, 3, 4) mm, can be calculated by using eqs. (2-26), (2-23) and (2-16), (2-15) and (2-57) as shown in figure (3-3). It is clear that the J_{th} decreases with increasing well width for each cavity length values where the best value is $J_{th} = 3743$ A/cm^2 which it is the same value at L=2mm, L=3mm, and L=4mm, when w=4.3nm and T=300K. After this value of J_{th}, it increases with increasing w.
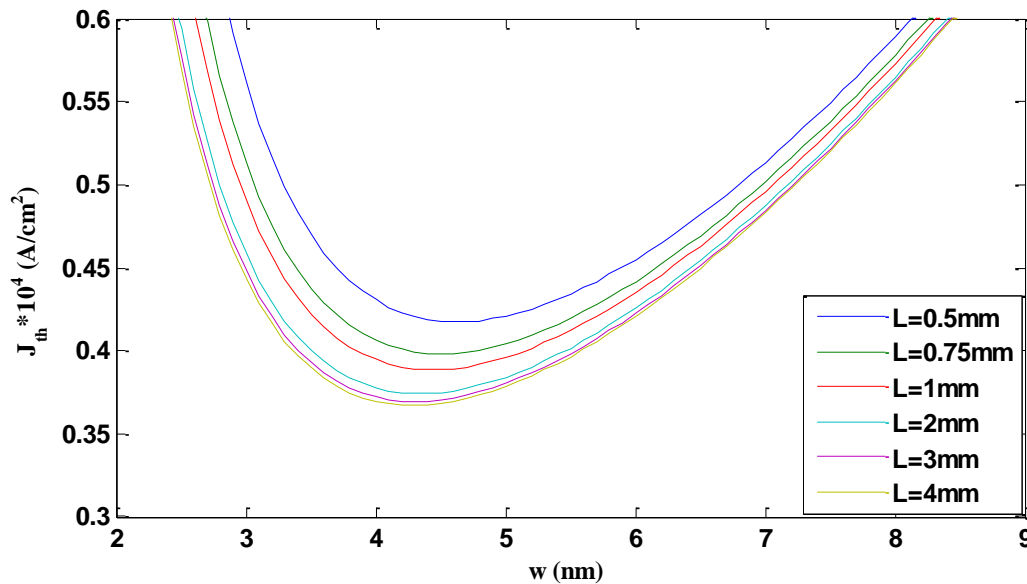

Figure (3-3): The threshold current density as a function of the well width for different cavity length.

Figure (3-4) shows that the threshold current density as a function of the well width (w) for several temperature values (77,150, 200, 250, 300) K, can be calculated by using equation (2-57). Interband transition occur between the conduction band and valence band, where electron transition of the one state (n=1) in conduction band to the one state (n=1) in the valence band (heavy hole (hh) or light hole (lh)), optical transition is allowed because $\Delta n = 0$. We note that the threshold current density decreases with increasing well width until it reaches the lowest value and then begins to increase. Figure (3-4a)

represents the threshold current density in case for TE mode of the electron transition must be from (n=1) in the conduction band (E_c) to (n=1) of light hole (lh) in the valence band (E_v) therefore used the momentum matrix element (*M*) eq (2-23) in eq. (2-19) and substituted it in eqs. (2-15) and (2-57). The lowest value of the threshold current density is J_{th}= 3743A/cm^2 at T=300K. Figure (3-4b) is the case for the TM mode of the transition occurs to the light hole (lh) level by used (*M*) eq. (2-23) in eq. (2-22) and substituted it in eqs. (2-15) and (2-57). The lowest value the threshold current density is J_{th}=3743A/cm^2 at T=300K. While figures (3-4c) and (3-4d) are representing the transitions occur to the heavy hole (hh) level for TE and TM modes respectively by substituted eq. (2-23) in eqs.(2-18) and (2-21) then in eqs. (2-15) and (2-57). Thus the lowest value of the threshold current density of these two transitions are J_{th}=2853A/cm^{2}and J_{th}=181.9A/cm^2 respectively. These values of threshold current density are obtained at w=4.3nm, T=300 K. Through the values of the J_{th}, it is clear that the lowest value of J_{th} is in the case of the figure (3-4d) where transition to hh level for TM modes due to that radiative recombination coefficient B$_{rad}$ =0.
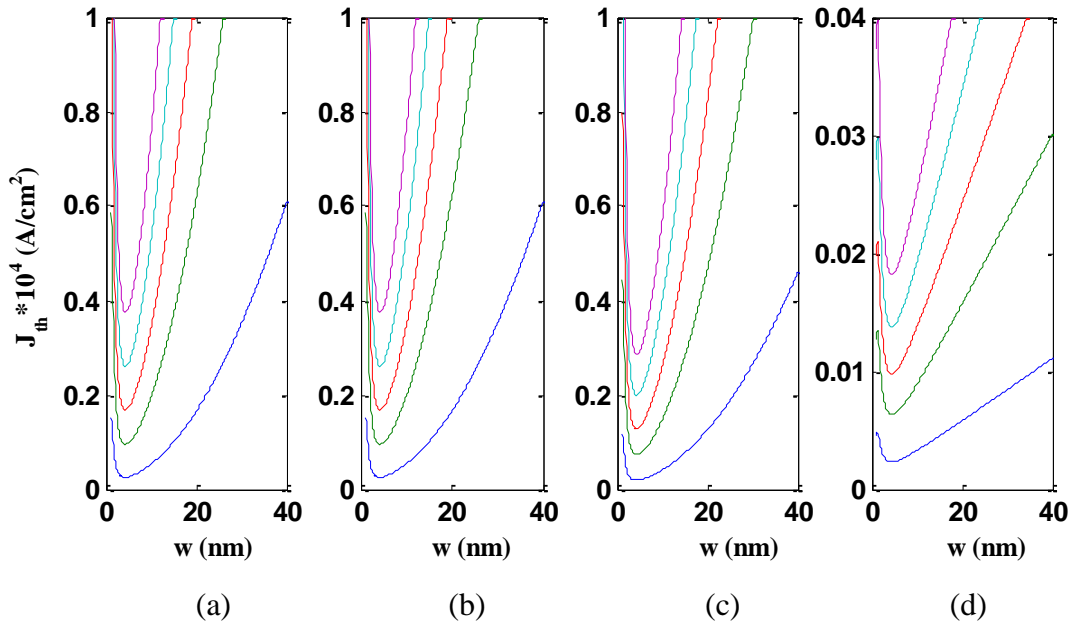

Figure (3-4): Threshold current density versus well width for the different temperature.
(a) TE mode for lh (b) TM mode for lh (c) TE mode for hh (d) TM mode for hh where
_____ T=77 K, _____ T=150 K, _____ T=200 K, _____ T=250 K, _____ T=300 K.

Figure (3-5) illustrates that the threshold current density versus well width w for several temperature (77,150, 200, 250, 300) K (from equation (2-57)). It is clear that the J_{th} decreases with increases well width until it reaches to the lowest value and then begins to increase for each value of temperature. Figure (3-5a) from equations (2-15), (2- 17), (2-18), (2-19), (2-23) and (2-57) for TE mode, and figure (3-5b) from eqs (2-15), (2-20) - (2-23) and (2-57) for TM mode. They are appear that the lowest value of the threshold current density is J_{th}= 258 A/cm^2 at T=77K and J_{th}= 3743 A/cm^2 at T=300K when w= 4.3nm.
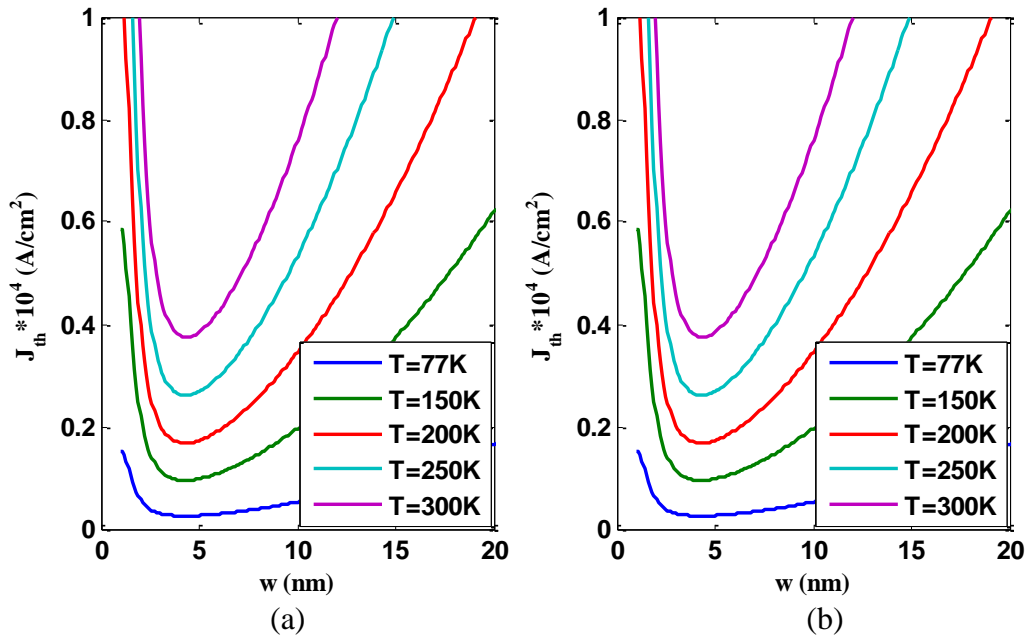

Figure (3-5): Threshold current density versus well width for the different temperature.
(a) TE mode   (b) TM mode

Equation (2-57) shows relation between the total threshold current density with well width (w) for several temperature T= (77,150, 200, 250, 300) K, as shown in figure (3-6) which was drawn by equations (2-15), (2-16) - (2-23) and (2-57). The lowest value of the threshold current density at T=77K is J_{th}= 258 A/cm^2 but at T=300K is J_{th}= 3743 A/cm^2 and w=4.3 nm.
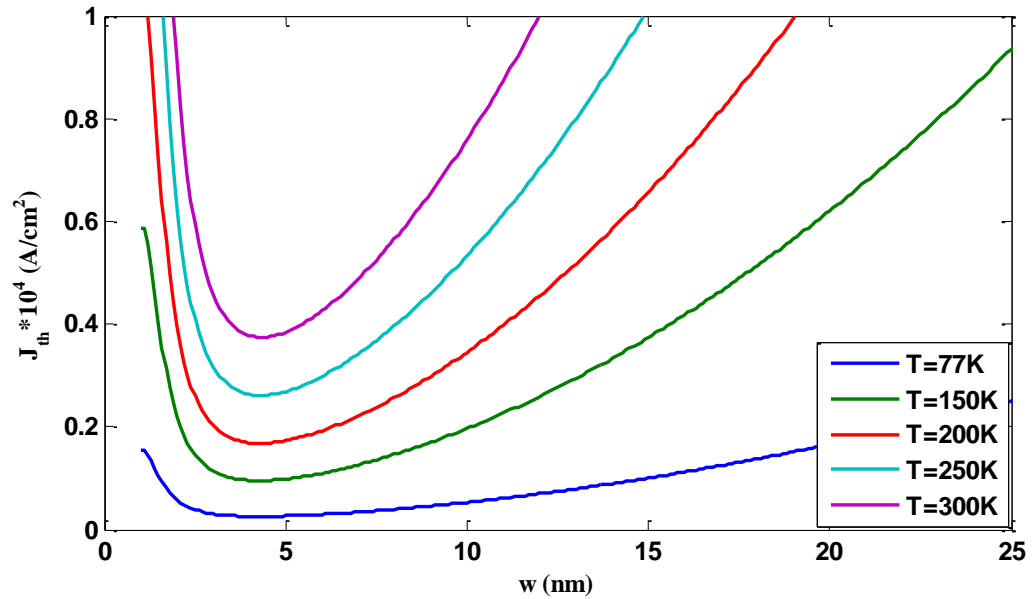
Figure (3-6): Threshold current density versus well width for the different temperature.

Figure (3-7) shows threshold current versus the well width (w) for different temperatures T=(77, 150, 200, 250, 300) K which can be calculated by using eq. (2-59). This figure shows that the behavior of threshold current curve is the same behavior with the threshold current density curve while the less value of the threshold current at T=77K is $I_{th} = 1.03$ mA but at T=300K is $I_{th} = 14.97$ mA and w=4.3 nm.
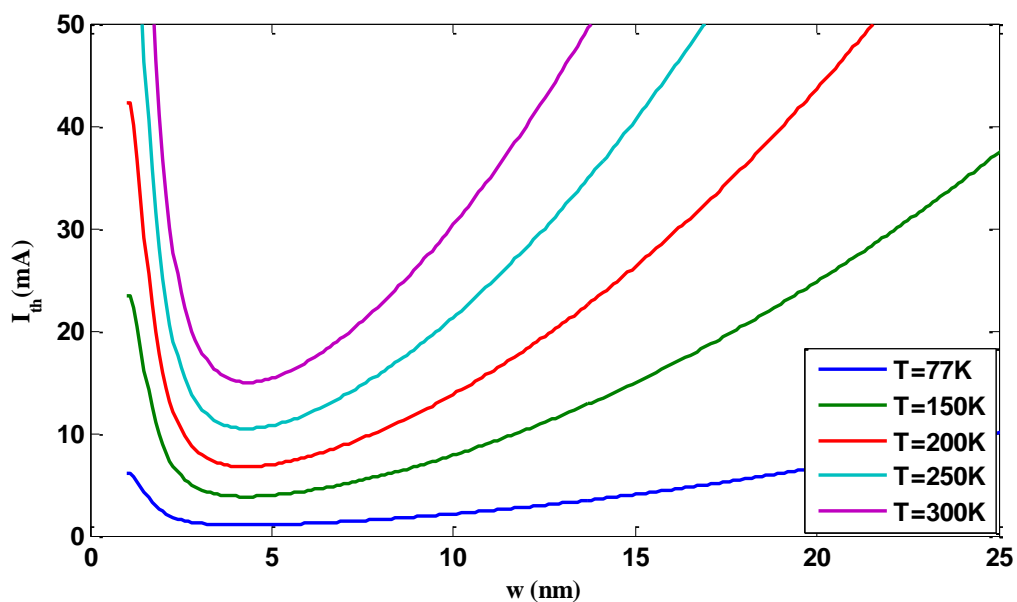

Figure (3-7): Threshold current versus the well width for different temperature.

3.4.2 Mirrors Reflectivity

The threshold current density versus the well width (w) for variations reflectivity R_1 and R_2 was calculated by using eq. (2-57), as shown in figure (3-8). This figure appears that the $J_{th} = 3743$ A/cm^2 when R_1=0.75 and R_2=0.9, as well as $J_{th} = 4840$ A/cm^2 when R1=R2=eq. (1-1), the threshold current density value is $J_{th} = 4256$ A/cm^2 when R_1=eq. (1-1) and R_2=0.9.Through these values, it is clear that the best value of threshold current density is 3743 A/cm^2 in the case reflectivity R_1=0.75 and R_2=0.9.
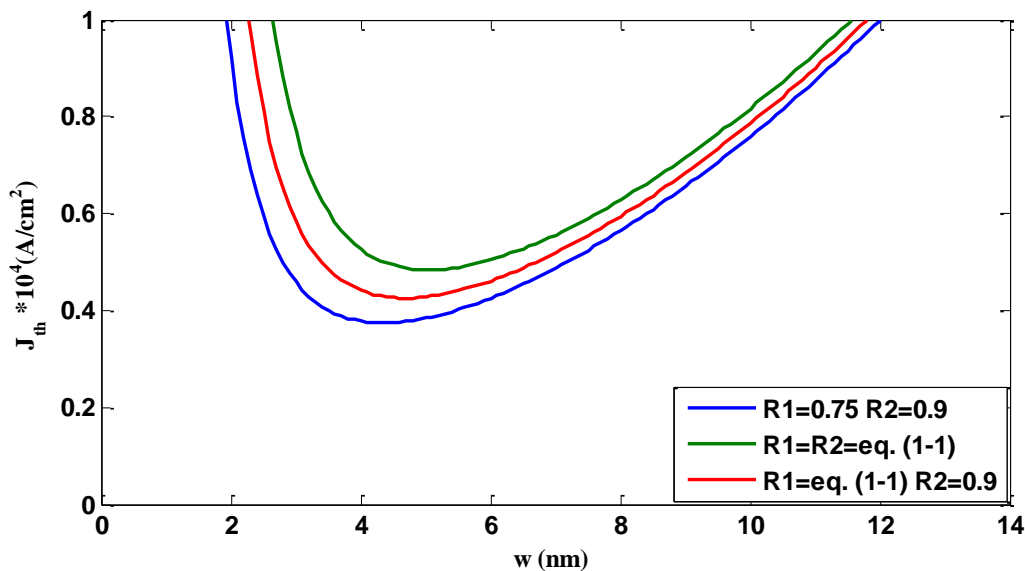

Figure (3-8): Threshold current density as a function of well width for different reflectivity.

Figure (3-9) show that the threshold current (I_{th}) versus (w) for various reflectivity's R_1 and R_2 was calculated by using eq. (2-59). This figure appears that the threshold current value is $I_{th} = 14.97$ mA when R_1=0.75 and R_2=0.9, also the threshold current density value is $I_{th} = 19.36$ mA when R_1=R_2=eq. (1-1) and the threshold current value is $I_{th} = 17.02$ mA when R1=eq. (1-1) and R2=0.9.Through these values, it is clear that the best value of threshold current is 14.97 mA in the case reflectivity R_1=0.75 and R_2=0.9.
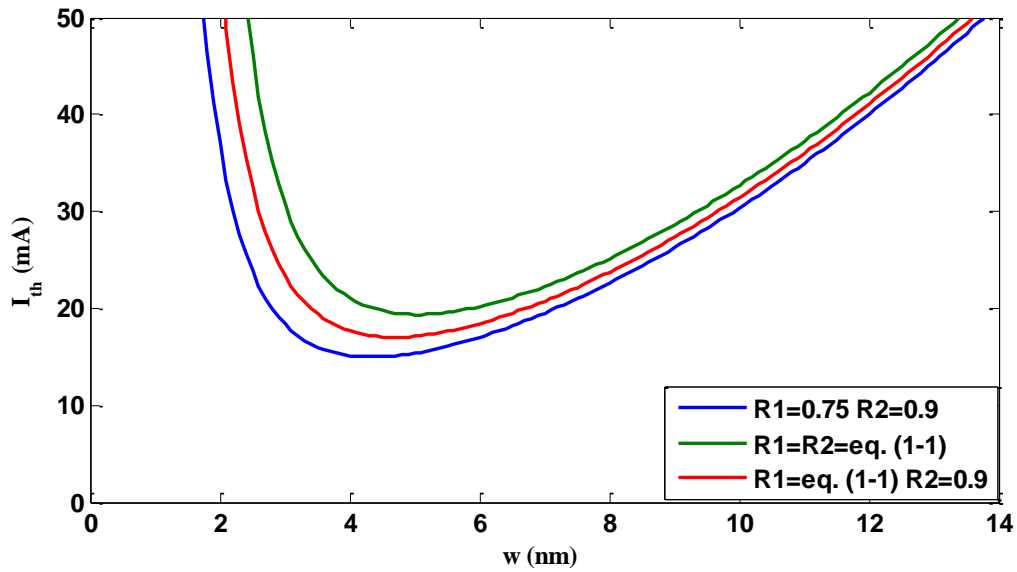
Figure (3-9): The threshold current versus the well width for different reflectivity.

3.4.3 Cavity Width (W)

Threshold current versus well width (w) for different cavity widths W= (200, 300, 400, 500, 600) nm can be calculated by eq. (2-59) as shown in figure (3-10). It is illustrate that the less value of the threshold current is $I_{th} = 14.97$mA when the well width is w= 4.3 nm and W=200 nm, it is the favorite value for the cavity width.
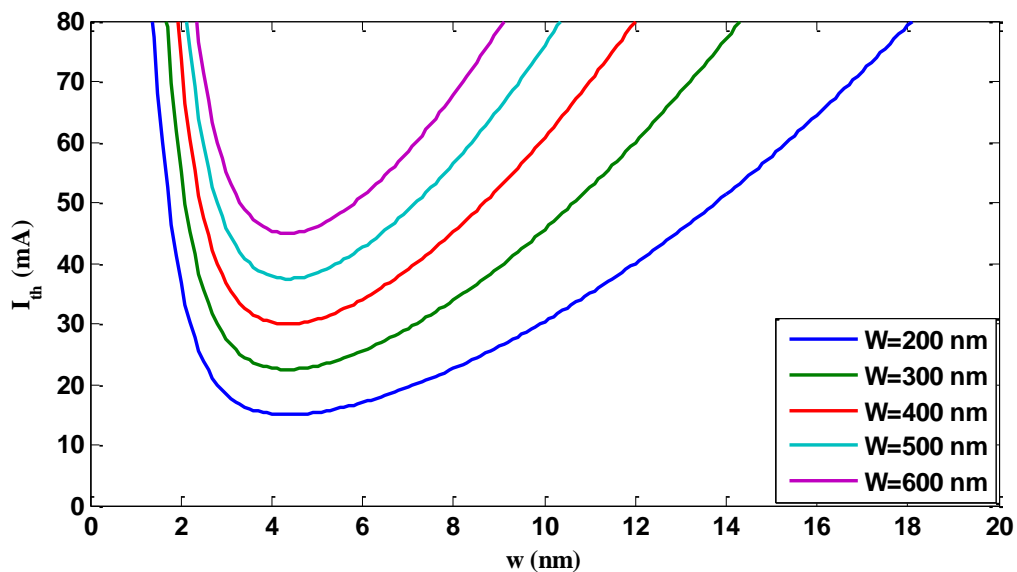

Figure (3-10): Threshold current as a function of well width for the different cavity width.

3.4.4 Average Thickness of Active Region (d)

The threshold current density as a function of the average thickness of active region (d) for different temperatures (77, 150, 200, 250, 300) K, can be calculated by using eq. (2-57) as shown in figure (3-11). It is clear that the J_{th} decreases with increasing average thickness of active region for each temperature value until the reach threshold current density to the lowest value is $J_{th} = 3743$ A/cm^2 at d = 10.6 nm and T=300K, then start increases.
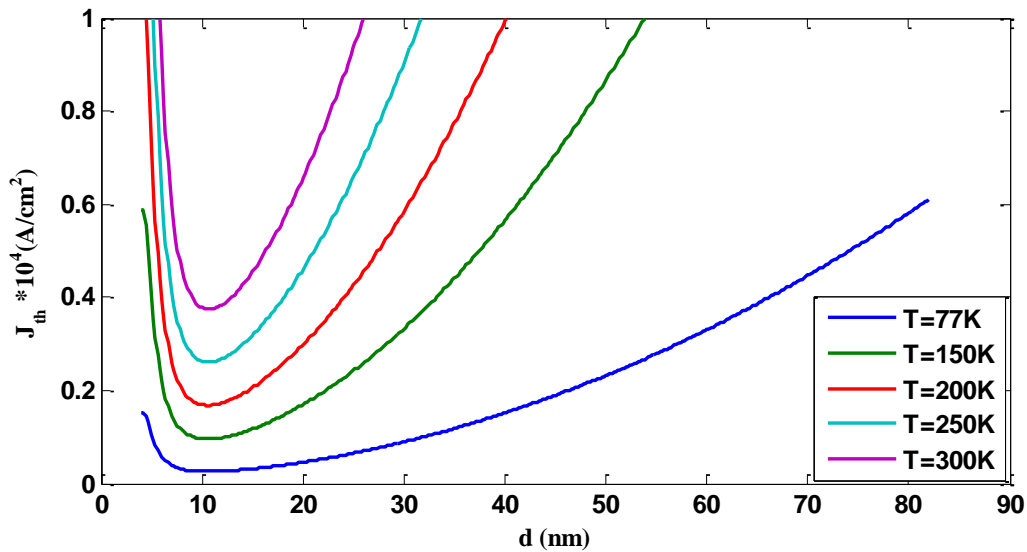

Figure (3-11): Threshold current density as a function of average thickness of active region for the different temperatures.

The threshold current as a function of the average thickness of active region (d) for different temperatures T= (77, 150, 200, 250, 300) K, can be calculated by using eq. (2-59) as shown in figure (3-12). It is clear that the lowest value of threshold current is $I_{th} = 14.97$ mA when d = 10.6 nm and T=300K, then start increases.

Through the previous figures for threshold current density and threshold current illustrate that both J_{th} and I_{th} increase with increasing temperature this is the increases cavity losses with increasing temperature. To overcome cavity losses we need more current to achieve the population inversion.
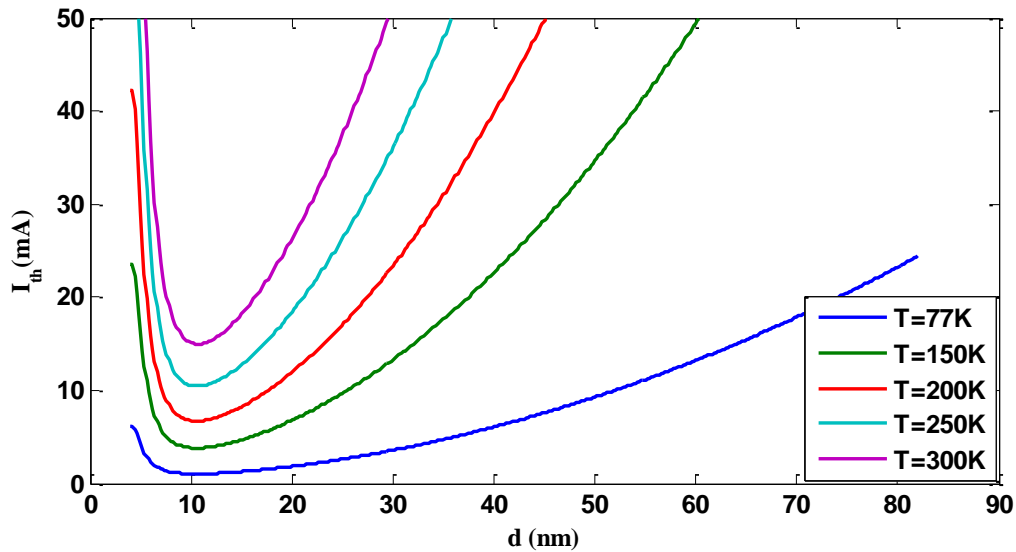
Figure (3-12): Threshold current as a function of average thickness of active region for the different temperatures.

3.4.5 Cavity Length (L)

The threshold current density versus the cavity length (L) for different values of temperature T= (70, 150, 200, 250, 300) is shown in figure (3-13), using equation (2-57). It clear that the threshold current density decreases with increases cavity length for each temperature values and then begin to be fixed almost near L=1 mm, this is because mode gain increased in a longer laser cavity. From this figure, the best value of threshold current density is $J_{th} = 3743$ Am/cm^2 when cavity length is L=2 mm and T=300 K.

Figure (3-13): Threshold current density as a function of cavity length for the different temperature.

Figure (3-14) shows that the threshold current versus the cavity length for different temperature T= (77, 150, 200, 250, 300) K, can be calculated by using equation (2-59). It shows a linear behaviors nature which suggests that the threshold current can be estimated at any cavity length, but the best value of threshold current is $I_{th} = 14.97$ mA at T=300K when L=2mm.

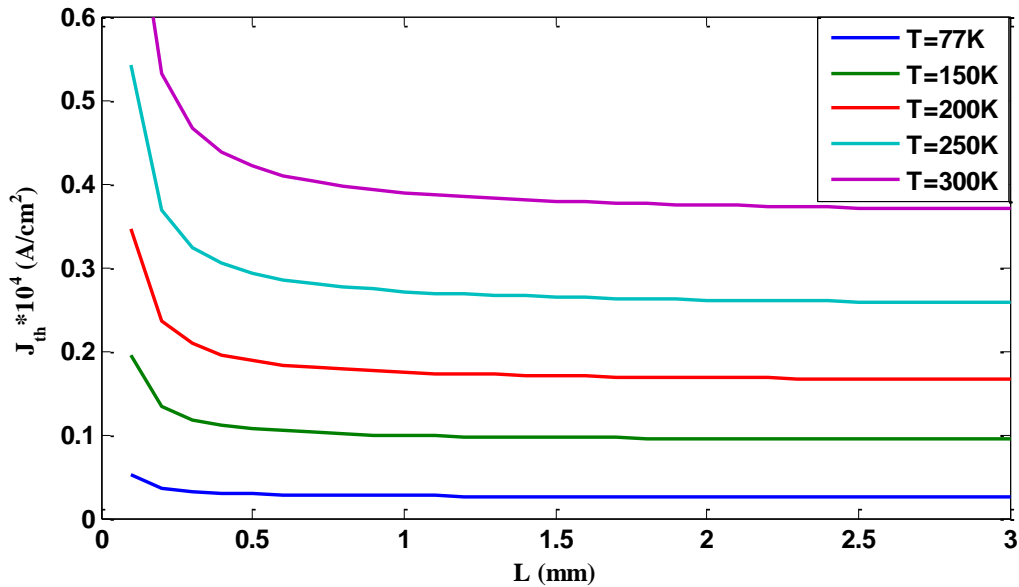**Figure (3-14):** Threshold current as a function of cavity length for the different temperature.

Figure (3-15) shows that the threshold current density as a function of the cavity length for different values of wells number N_w= (2, 4, 6) was calculated by using eq. (2-57). It is shown that the threshold current density decreases with increasing cavity length for each number of wells values and then begin constant near L=1 mm, that the best value of $J_{th} = 3743$ A/cm^2 when cavity length is L=2 mm and $N_w = 2$.

Figure (3-15): Threshold current density as a function of cavity length for the different number of wells.

Figure (3-16) shows that the threshold current as a function of the cavity length for several wells number N_w= (2, 4, 6), can be calculated by using equation (2-59). The curve of the threshold current in a straight line, the lowest value of Threshold current is $I_{th} = 14.97$ mA when L=2mm and $N_w = 2$.
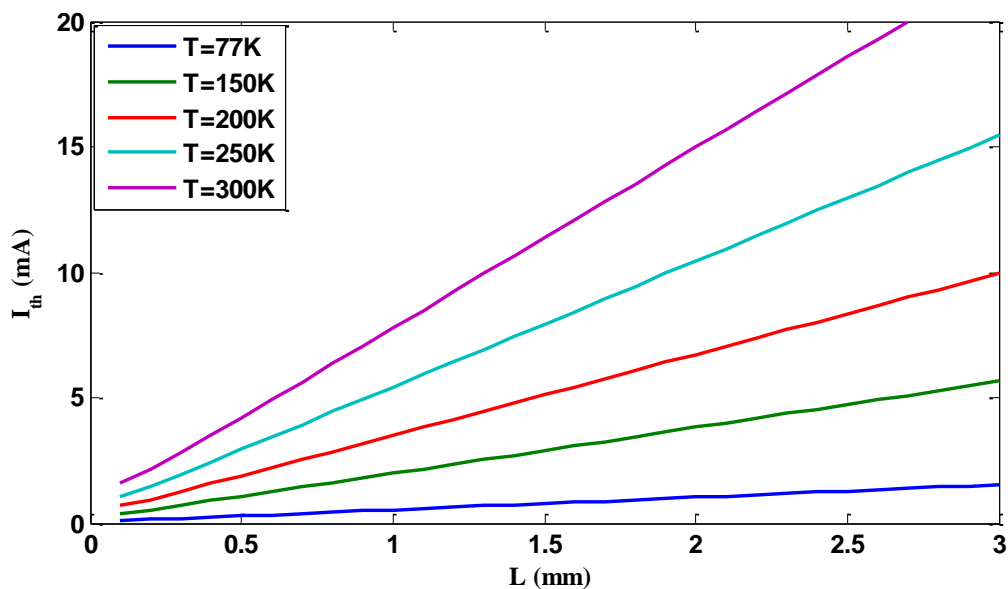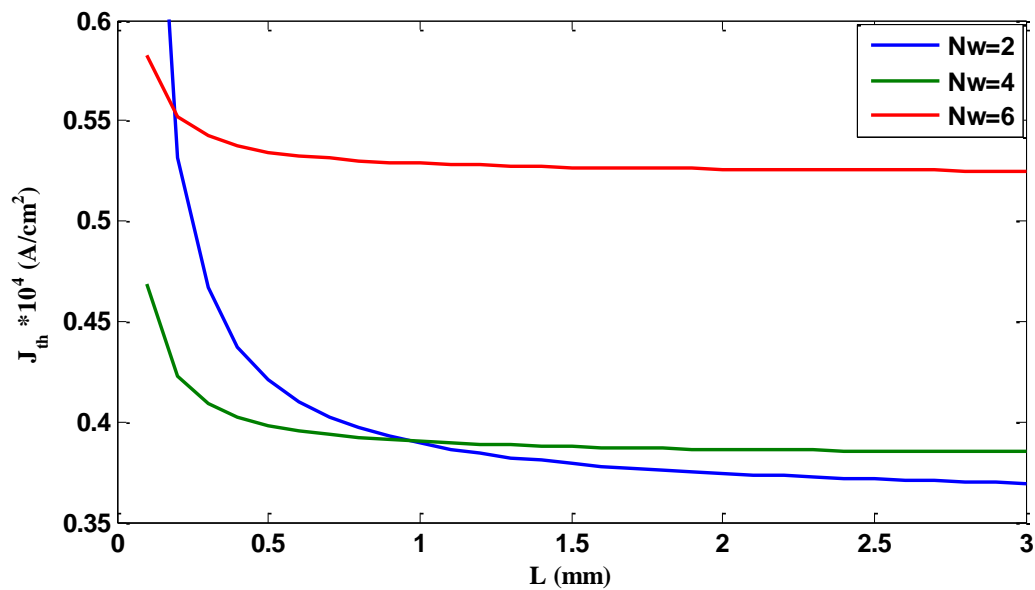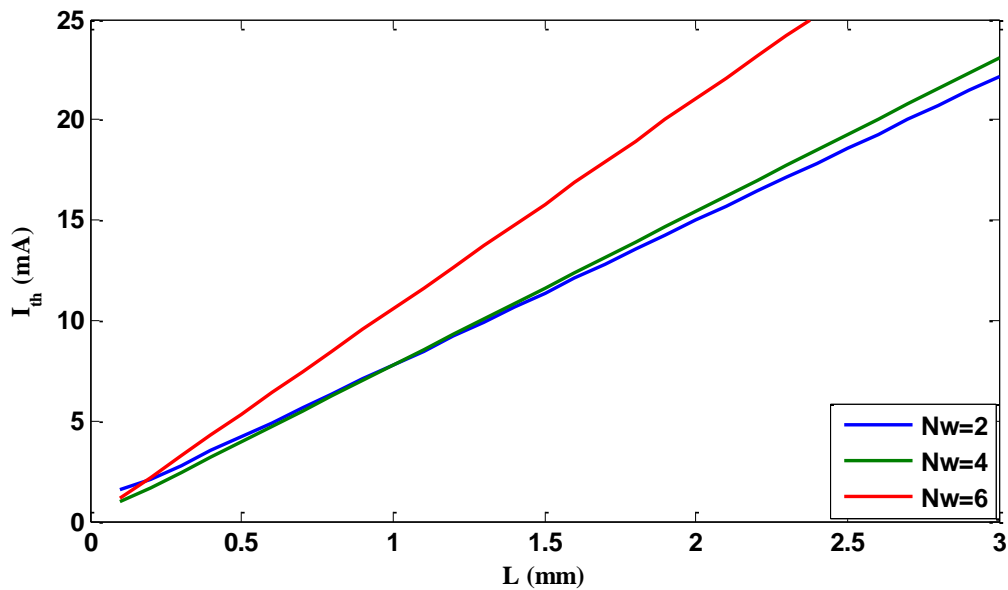
Figure (3-16): Threshold current as a function of cavity length for the different number of wells.

The threshold current density as a function of the cavity length for different reflectivity of cavity mirrors (R_1, R_2) as shows in figure (3-17), was calculated by equation (2-57). It indicates that the threshold current density decreases with increasing cavity length and it begins constant near L=1mm, that the value the threshold current density $J_{th} = 3743$ A/cm^2 when R_1=0.75 and R_2=0.9, so $J_{th} = 5034$ A/cm^2 when R1=R2=eq. (1-1), and $J_{th} = 4302$ A/cm^2 when R1=eq. (1-1) and R2=0.9. Through the values of the threshold current density noted that the lower value is $J_{th} = 3743$ A/cm^2 when R_1=0.75, R_2=0.9 and T=300 K.
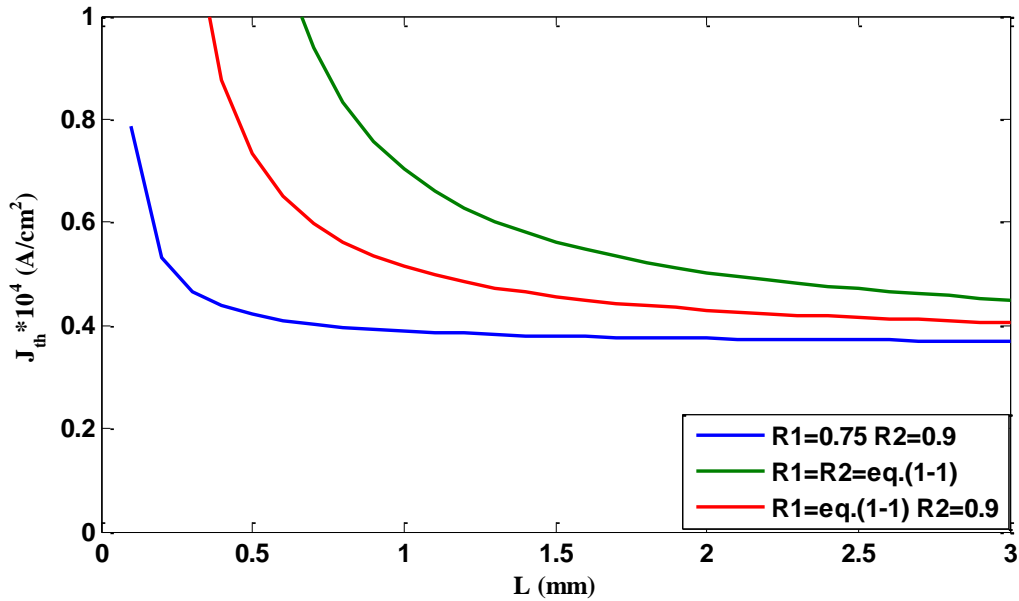
Figure (3-17): Threshold current density as a function of cavity length for the different reflectivity.

3.4.6 Mirror Loss (α_m)

The threshold current density as a function of the mirror loss was calculated by using eq. (2-57), as shown in figure (3-18). Through this figure noted that the threshold current density increase with increasing mirror loss until it reach to the value of mirror loss α_m=0.98 cm^{-1} when the threshold current density J_{th}= 3743 A/cm^2 and T=300 K, R$_1$=0.75 and R$_2$=0.9.
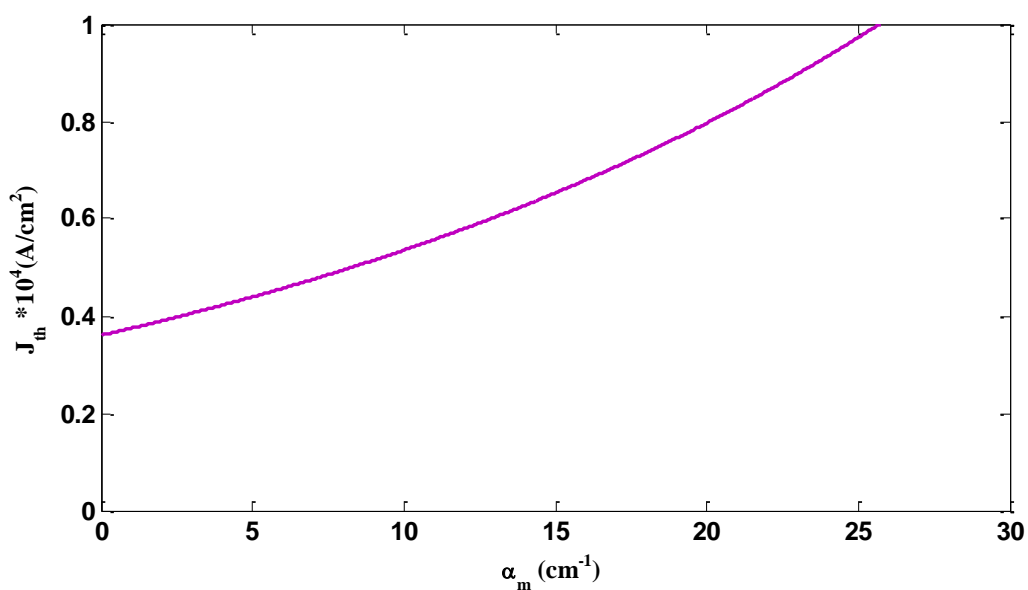
Figure (3-18): Threshold current density versus mirror loss.

Figure (3-19) shows that the dependence of threshold current on the mirror loss which calculated by using eq. (2-59), this figure shows that the threshold current increase with increasing mirror loss until it reach to the value of mirror loss α_m=0.98 cm^{-1} at the threshold current value I_{th}= 14.97 mA and T=300 K.
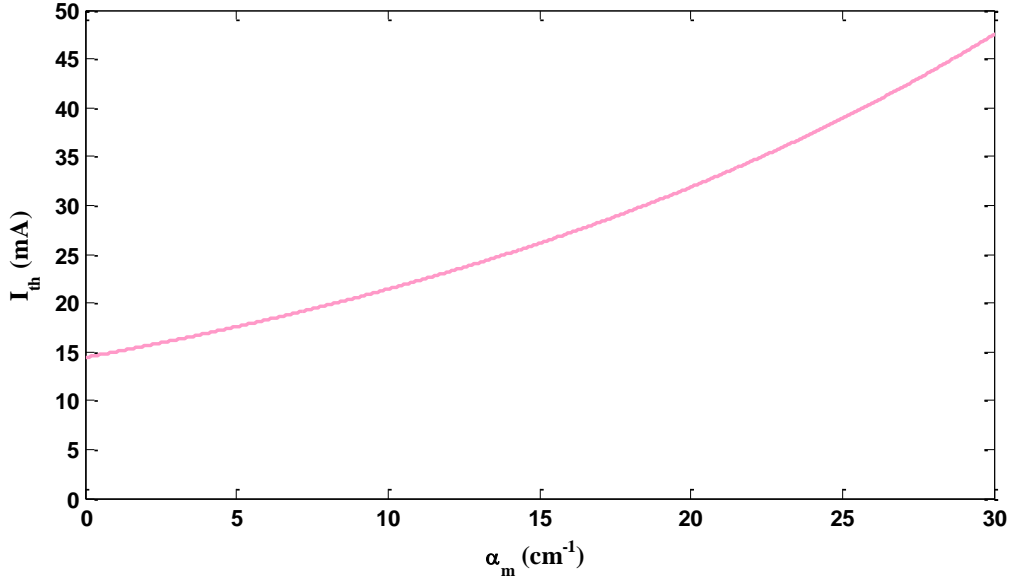
Figure (3-19): Threshold current as a function of mirror loss.

3.4.7 Threshold Gain (g_{th})

Threshold current density versus the threshold gain was calculated by using equation (2-57) as shown in figure (3-20), it is clear that the threshold current density increases exponentially with increasing threshold gain. When the threshold current density is J_{th}= 3743 A/cm^2, the threshold gain is g_{th} = 791 cm^{-1}.
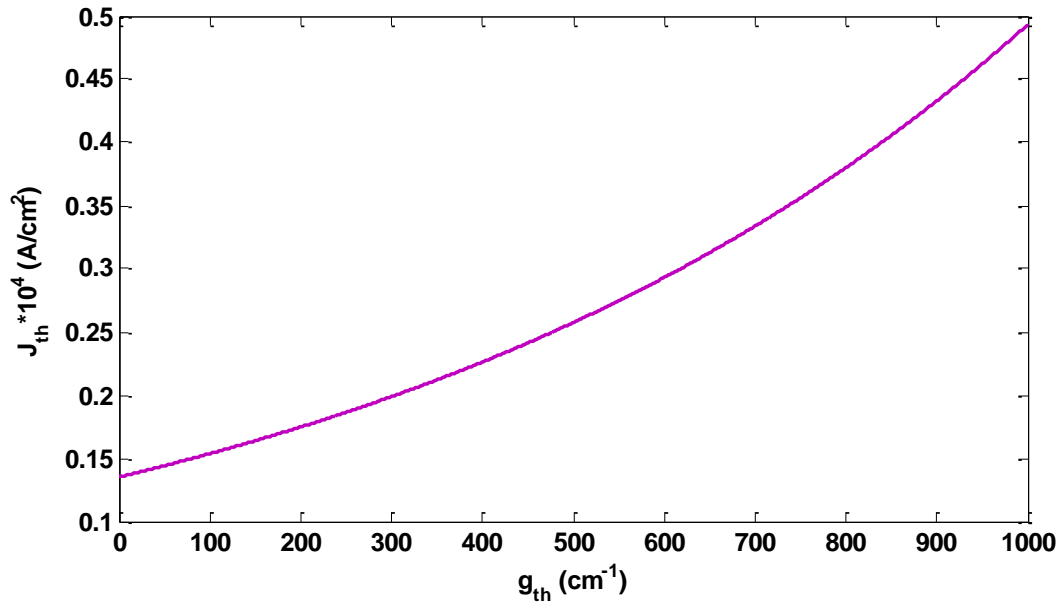
Figure (3-20): Threshold current density versus threshold gain.

Figure (3-21) illustrates that the dependence of threshold current on the threshold gain was calculated by using eq. (2-59). This figure show that threshold current increases with increasing threshold gain. The threshold gain value is $g_{th} = 791$ cm^{-1}, when the threshold current is $I_{th} = 14.97$ mA.
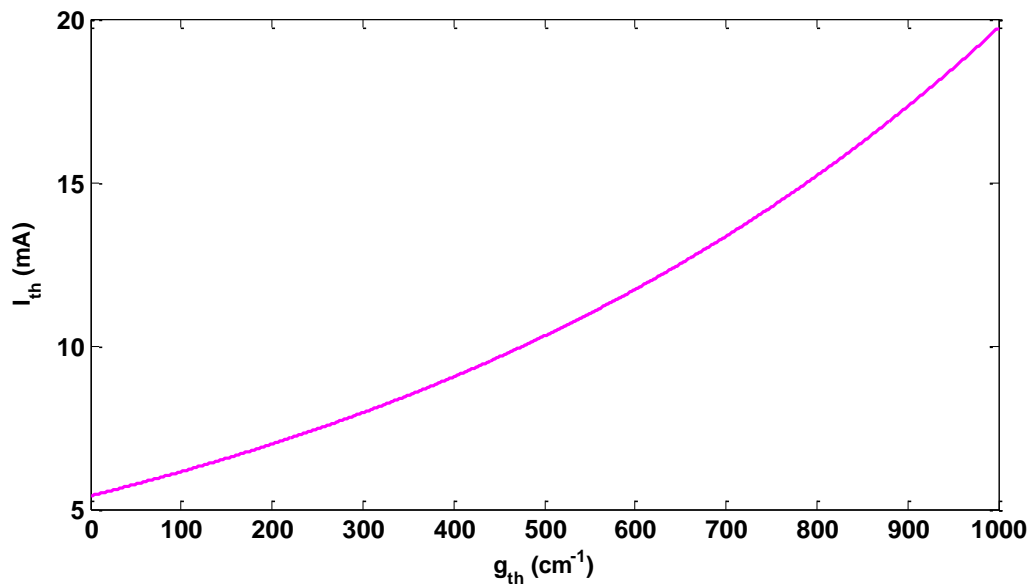
Figure (3-21): Threshold current as a function of threshold gain.

CHAPTER FOUR

CONCLUSION AND FUTURE WORK

4.1 Conclusion

In conclusion, $Al_{0.01}Ga_{0.99}N$/GaN multiple quantum well laser structure emitted wavelength of 352 nm which is within the long UV (UVA) range. This system shows that the optical confinement factor increases with increasing well widths. The best value of the optical confinement factor is 0.4107 when number of wells N_w=2 and barrier width (b=2nm) is the smallest barrier width. From these results appear that the optical confinement factor is the important factor to determine the parameters of this structure.

The parameters which effecting on the threshold current density and threshold current was determined to obtain the optimum values of threshold current density ($J_{th} = 3743$ A/cm^2) and threshold current ($I_{th} = 14.97$ mA) such as: well width (w), average thickness of active region (d),cavity length (L), mirror loss(α_m) and threshold gain (g_{th}).Those parameters can be inserted by table (4-1).

Table (4-1): The results values for Al$_{0.01}$Ga$_{0.99}$N/GaN multiple quantum well laser T=300K.

Parameters	Symbol	Values	Unit
Threshold current density	J_{th}	3743	A/cm^2
Threshold current	I_{th}	14.97	mA
Well width	w	4.3	nm
Average thickness of active region	d	10.6	nm
Cavity width	W	200	nm
Reflectivity coefficient the first mirror	R$_1$	0.75	Non
Reflectivity coefficient the two mirror	R$_2$	0.9	Non
Cavity length	L	2	mm
Mirror loss	α_m	0.98	cm^{-1}
Threshold gain	g_{th}	791	cm^{-1}

4.2 Suggestions for Future Work

1- Theoretical optimization of threshold current InGaN/GaN and AlGaAs/GaAs for multiple quantum well lasers and compared with AlGaN/GaN

2- Theoretical optimization of threshold current for semiconductor materials emitting laser in infrared range.

3- A study AlGaN/GaN for quantum wire laser and quantum dot laser.

References

1- E. Kapon, **Semiconductor Lasers I Fundamentals**, optics and photonics, Academic Press, p. 1, (1999).

2- H. G. -Shiraz, **The Principles of Semiconductor Laser Diodes and Amplifiers**, Imperial College Press, p. 361, (2004).

3- J. N. Blakely, **"Experimental Control of A Fast Chaotic Time Delay Optoelectronic Device"**, Department of Physics Duke University, (2003).

4- S. M. Sze, **physics of semiconductor devices**, 3rd Edition, pp. (602, 611), (2007).

5- M. Fukuda, **Optical Semiconductor Devices**, Wiley Series in Microwave and Optical Engineering Kai Chang, p. 93, 1999.

6- M. Kebede, **"Low Lying Energy States of two Electron Quantum Dots with Rigid Confinement"**, Addis Ababa University, (2011).

7- G. Schmid, **Nanoparticles: From Theory to Applications**, 2nd Edition, Wiley-VCH-Verleg GmbH and Co.KGaA, (2010).

8- X. Liu, W. Zhao, L. Xiong and H. Liu, **Packaging of High Power Semiconductor Lasers**, Springer Science - Business Media New York, pp. (3-6), (2015).

9- T. Numai, **Laser Diodes and Their Applications to Communications and Information Processing**, John Wiley & Sons, Inc., pp. (15, 26-29, 47-48, 191-192, 197-199), (2010).

10- H. A. Makarimi, **"Threshold Current Temperature Dependence of Indium Phosphide Quantum Dot Lasers"**, Cardiff University, (2014).

11- A. Ghatak, **Optics**, 4thEdition, Tata McGraw-Hill Education, ch26 pp. (1,5), (2009).

12- E. Simpson, **"The Basic Principles of Laser Technology Uses and Safety Measures in Anaesthesia"**, University Trust, March (2012).

13- E. K-Asibu, **Principles of Laser Materials Processing**, a John Wiley, Sons, Inc., Publication, pp. (19, 20, 160), (2009).

14- J. Ohtsubo, **Semiconductor Lasers**, 2nd Edition, Springer Series in Optical Sciences, p.25, (2008).

15- L. Jiang, **"Theoretical Study of Performance Characteristics of Semiconductor Quantum Dot Lasers"**, State University, (2008).

16- T. L. Floyed, **Electronic Devices: Conventional Current Version**, 8th Edition, (2008).

17- D. A. Neamen, **Semiconductor Physics and Devises Basic Principle**, the McGraw-Hill Companies, New York, 4th Edition, p.(243-244), (2012).

18- S. Kumar and M. J. Deen**, Fiber Optic Communications: Fundamentals and Applications**, Wiley, p. 119, (2014).

19- S. S. Li, **Semiconductor Physical Electronics**, 2nd Edition, Springer Science –Business Media, LIC, p.341, (2006).

20- O. Svelto, **Principles of Lasers**, 5th Edition, Springer Science –Business Media, LIC, p.407, (2010).

21- J. Hecht, **Understanding Lasers**, 3^{ed} Edition, IEEE Press Understanding Science and Technology Series, pp. (282-283), (2008).

22- M. Csele, **Fundamentals of Light Sources and Lasers**, John Wiley & Sons, Inc, pp. 315, (2004).

23- J. F. Donnelly and N. M. Massa, **Light: Introduction to Optics and Photonics**, The New England Borad of higher Education, p. 225, (2007).

24- C. Jacoboni and P. Lugli, **"The Monte Carlo Method for Semiconductor Device Simulation"**, Springer -Verlag Wien, New York, p. 86, (1989).

25- Y. O. Yilmaz, **"External Wavelength stabilization of Grating Coupled Surface Emitting Lasers and Applications"**, The University of North Carolina at Charlotte, (2012).

26- J-M. Liu, **Photonic Devices**, Cambridge University Press, pp. (613,821, 838-839, 846), (2005).

27- B. E. Gihleengen, L. Thoresen and K. A. Grimsrud, **Semiconductor Lasers**, TFY14 Functional Materials-NTNU, (2007).

28- J. Hill, **"Lasers Diode Technology and Applications"**, Protland State University Physics, (2005).

29- W. Nagourney, **Quantum Electronics for Atomic Physics**, Oxford University Press, p. 163, (2010).

30- Z. Alferov, **"Double Heterostructure Lasers: Early Days and Future Perspective"**, IEEE Journal on Selected Topics in Quantum Electronics, Vol.6, No. 6, (2000).

31- T. K. Abd Al-Raheem,**"Ab-Initio Study the Electronic Structure of $In_xGa_{1-x}P$ Nanocrystals"**, University of Baghdad College of Science, (2013).

32- N. A. Cukaric, **"Modelling the Electron and Hole States in Semiconductor Nanostructure by Multiband k.p Theory"**, university of Belgrade, (2015).

33- J. M. Martinez-Duart, R. J. Martin-Palma and F. Agullo-Rueda, **Nanotechnology for Microelectronics and Optoelectronics**, Elesvier B.V., (2006).

34- A.Irrera, Ph. D. Thesis **"Light Emitting Devices based on Silicon Nano structures"**, Universita Degli Studi Di Catania, (2003).

35- F.Charra and S.Gota-Goldmann, **"Mesoscopic and Nanostructured Materials"** Part5, Springer Berlin Heidelberg, (2005).

36- M. Razeghi, **Fundamental of Solid State Engineering**, 3rd Edition, Springer Science-Business Media, pp. (88, 101, 499, 501, 508, 509, 513), (2009).

37- Y. Aoyagi and K. Kajikawa, **Optical Properties of Advanced Materials**, Springer Series in Materials Science, Vol. 168, pp. (12, 14-18), (2013).

38- O.Manasreh, **Semiconductor Heterojunctions and Nanostructures**, McGraw-Hill Nanoscience and Nanotechnology Series, pp. (166-168, 171-173), (2005).

39- G. L. Oppo, S. M. Barnett, E. Riis and M. Wilkinson, **Quantum Dynamics of Simple Systems**, The Scottish Universities summer Scholl in Physics, p. 240, (1996).

40- D. A. Anghel, A. R. Sterian and P. E. sterian, **"Modeling Quantum Well Lasers"**, Hindawi Publishing Corporation Mathematical Problems in Engineering, p. (1-11), (2012).

41- J. E. Nkanta, **"Modeling and Characterization of Laterally-Coupled Distributed feedback laser and Semiconductor optical Amplifier"**, University of Ottawa, Canada, (2016).

42- X. Wen, **"Ultrafast Spectroscopy of Semiconductor Nanostructures"**, University of Technology, Melbourne, Australia, (2007).

43- M. Zaluzny,**"Intersubband Transitions in n-type quantum well systems"**, Opto-Electronics Review, Vol. 7, No. 2, pp. (81-86), (1999).

44- J. M. Senior, **Optical Fiber Communications Principles and Practice**, 3rd Edition, Pearson Education Limited, p. 339, (2009).

45- S. Kasap and P. Capper, **Springer Handbook of Electronic and Photonic Materials**, Springer Science-Business Media, Inc., pp. (57-58), (2006).

46- C. R. King and Jr. Georgia, **"Density of States 2D, 1D and 0D"**, Introduction to Microelectronics Theory December 17, Lecture Prepared, (2005).

47- M. Kuno, **Introductory Nanoscience: Physical and Chemical Concepts**, Garland Science, (2012).

48- H. Zappe, **Laser Diode Microsystems**, Springer Verlag Berlin Heidelberg Gmbh, pp. (67, 69-70, 92), (2004).

49- D. S. patil, **Semiconductor Laser Diode Technology and Application**, Published InTech, pp. (13, 16-17), (2012).

50- Q. Wang, **"Development of enhancement-mode GaN MOSFET on AlGaN/GaN heterostructure"**, Tokushima University, (2015).

51- I. Vurgaftman, J. R. Meyer and L. R. Ram-Mohan, **"Band Parameters for III-V Compound Semiconductor and Their Alloys"**, J. Appl. Phys. Rev., Vol. 89, No. 11, (2001).

52- H. Morkoc, **Handbook of Nitride Semiconductors and Devices**, Vol. 1: Materials Properties, Physics and Growth, Wiley-VCH-Verleg GmbH and Co.KGaA, Weinheim, pp. (18, 19, 27, 90), (2008).

53- N. Nepal, J. Li, M. L. Nakarmi, J. Y. Lin and H. X. Jiang, **"Temperature and Compositional Dependence of The Energy Band Gap of AlGaN Alloys"**, Appl. Phy. Lett., Vol. 87, p. 242104, (2005).

54- J. Piprek, R. K. Sink, M. A. Hansen, J. E. Bowers and S. P. Den Baars, **"Simulation and Optimization of 420 nm InGaN/GaN Laser Diodes"**, Physics and Simulation of Optoelectronic Devices VIII, pp. (1-12), (2000).

55- H. -H. Park and B. -S. Yoo, **"Low Threshold Current Density and High Efficiency Surface Emitting Lasers with a Periodic Gain Active Structure"**, ETRI Journal, Vol.17, No.1, (1995).

56- W. J. Fan, M. F. Li and T. C. Chong, **"Valence Hole Subbands and Optical Gain Spectra of GaN/Ga$_{1-x}$Al$_x$N Strained Quantum Wells"**, J. Appl. Phys., Vol. 80, No. 6, pp. (3471-3478), (1996).

57- Y. C. Yeo, T.C. Chong, M. F. Li and W. J. Fan, **"Analysis of Optical Gain and Threshold Current Density of Wurtzite InGaN/GaN/AlGaN Quantum Well Lasers"**, J. Appl. Phys. Vol. 84, pp. 1813-19, (1998).

58- S. Nakamura, M. Senoh, S.-i. Nagahama, N. Iwasa, T. Yamada, T. Matsushita, H. Kiyoku, Y. Sugimoto, T. Kozaki and H. Umemoto, **"InGaN/GaN/AlGaN-Based Laser Diodes Grown on GaN Substrates with a Fundamental Transverse Mode"**, Japanese Journal of Applied Physics, Vol. 37, Part 2, No. 9A/B, (1998).

59- S. R. Selmic, T.-M. Chou, J. Sih, J. B. Kirk, A. Mantie, J. K. Butler, D. Bour, and G. A. Evans, **"Design and Characterization of 1.3 m AlGaInAs-InP Multiple Quantum Well Lasers"**, IEEE Journal on Selected Topics in Quantum Electronics, Vol. 7, No. 2, pp. (16-19), (2001).

60- N. Tansu and L. J. Mawst, **"Current Injection Efficiency of InGaAsN Quantum-Well Lasers"**, J. Appl. Phys., Vol. 97, 054502, pp. (1-18), (2005).

61- K. Hild, S. J. Sweeney, S. Wright, D. A. Lock, S. R. Jin, I. P. Marko, S. R. Johnson, S. A. Chaparro, S. Q. Yu, and Y. H. Zhang, **"Carrier Recombination in 1.3 µm GaAsSb/GaAs Quantum Well Lasers"**, Appl. Phys. Lett., Vol. 89, 173509, pp. (1-3), (2006).

62- Y. -K. Ee, P. Kumnorkaew, R. A. Arif, J. F. Gilchrist, and N. Tansu, **" Enhancement of Light Extraction Efficiency of InGaN Quantum Wells Light Emitting Diodes Using SiO$_2$/Polystyrene Microlens arrays"**, Appl. Phys. Lett., Vol. 91, No. 22, 91, 221107, pp.(1-3), (2007).

63- H. Zhao, R. A. Arif, Y. -K. Ee, N. Tansu, **"Optical Gain Analysis of Strain-Compensated InGaN-AlGaN Quantum Well Active Regions for Lasers Emitting at 420-500 nm"**, Opt. Quant. Electron, pp. (301-306), (2008).

64- H. Yoshida, M. Kuwabara, Y. Yamashita, Y. Takagi, K. Uchiyama and H. KaN, **"AlGaN-Based Laser Diodes for the Short Wavelength Ultraviolet Region"**, New Journal of Physics, Vol. 11, 125013, pp. (1-14), 2009.

65- A. I. Hassan, **"A Theoretical Study of the Dynamical Behavior of SQW GaAs/AlGaAs Laser"**, Eng. &Tech. Journal, Vol. 28, No. 20, (2010).

66- H. Fatima, B. Abderrahmane and H. Abderrachid, **"Performance Characteristics of GaAs/ $Al_{0.32}Ga_{0.68}As$ Quantum Well Lasers"**, Sensors & Transducers, Vol.192, Issue 9, pp. (90-95), (2015).

67-69- M. Khodr, **"Quantum Efficiency Effects on Modal Gain, Threshold and Threshold Current Density of PbSe / $Pb_{0.934} Sr_{0.066}$ Se Multiple Quantum Well Structure"**, Res. J. Appl. Sci. Eng. Techol., Vol. 12, No. 5, pp.(607-611), (2016).

68- B. G. Yacobi, <u>**Semiconductor Materials an Introduction to Basic Principles**</u>, MICRODEVICES Physics and Fabrication Technology, pp. (35-39), (2004).

69- A. C. Melissinos and J. Napolitano, **Experiments in Modern Physics**, 2nd Edition, Content Technologies, Inc, (2017).

70- A. Tashtush, **"Characterization of Integration Bragg gratings in silicon on-insulator"**, University of Bologna, (2015).

71- S. Khanna and S. Nivedita**, "Recombination of Charge Carriers in p-n Junction Semiconductor"**, IJIRT, Vol. 1, Issue 6, pp. (1659-1662), (2014).

72- Lecture 17, generation/ Recombination, September (2000).

73- B. A. Ikyo, **"Electron Hole and Photon Recombination Processes in Quantum Well Semiconductor Lasers"**, American Journal of optics and photonics, Vol. 3, No. 5, pp. (80-84), (2015).

74- B. Gonul and M. Oduncuoglu, **"A Theoretical Comparison of the Pressure Dependence of the Threshold Current of Phosphorus-Aluminium- and Nitrogen-Based 1.3 μm Lasers"**, Semicond. Sci. Technol., 19, pp. (23-32), (2004).

75- H. Zhao, G. Liu, J. Zhang, R. A. Arif and N. Tansu**, "Current Injection Efficiency Induced Efficiency Droop in InGaN Quantum Well Light-Emitting Diodes"**, Solid-State electronics, Vol. 54, No. 10, pp. (1119-1124), (2010).

76- C. Hamaguchi, **Basic Semiconductor Physics**, Springer Verlag Berlin Heidelberg New York, p. 475, (2001).

77- H. Zhao, R. A. Arif and N. Tansu, **" Design Analysis of Staggered InGaN Quantum Light Emitting Diodes at 500-540 nm"**, IEEE

Journal of Selected Topics in Quantum Electronics, Vol. 15, No. 4, pp. (1104-1114), July/August, (2009).

78- J.-H. Yang, L. Shi, L. -W. Wang and S. –H. Wei, **"Non-Radiative Carrier Recombination Enhanced by Two Level Process; A First Principles Study"**, Scientific Reports 6, Article number: 21712, pp. (1-10), (2016).

79- E. F. Schubert, **light-Emitting Diodes**, 2nd Edition, Cambridge University Press, Cambridge New York, p. 40, (2006).

80- M. D. Laurentis and A. Irace, **"Optical measurement techniques of recombination lifetime based on the free carriers absorbation effect"**, Journal of solid state physics, pp. (1-19), (2014).

81- R. R. Hasan and R. Basak, **"Characteristics of a Designed 1550 nm AlGaInAs/InP MQW VCSEL"**, International Journal of Multidisciplinary Sciences and Engineering, Vol. 4, No. 1, pp. (5-9), (2013).

82- D. Vasileska, **Cutting Edge Nanotechnology**, In-Tech, p. 285, (2010).

83- E. F. Schubert, **Physical Foundations of Solid-State Devices**, New York, Ch.12, pp. (13-14), (2006).

84- S. Q. Mawlud, **"Bias Voltage Dependence on Thermoelectric Cooler Coefficient for Al$_{0.7}$Ga$_{0.3}$As and In$_{0.2}$Ga$_{0.8}$As SQW Laser Diode"**, Tikrit Journal of Pure Science, Vol. 16, No.4, (2011).

85- Y.-Z. Huang, Z. Pan and R.-H. Wu, **"Analysis of the optical confinement factor in semiconductor lasers"**, Journal Applied Physics, Vol. 79, No. 8, pp. (3827-3830), (1996).

86- M. F. Khodr, P. J. McCann and B. A. Mason, **"Optimizing and Engineering EuSe-PbSe$_{0.78}$Te$_{0.22}$-EuSe Multiple Quantum Well Laser Structures"**, IEEE Journal of Quantum Electronics, Vol. 34, No. 9, pp. (1604-1611), (1998).

87- J. Piprek, **Semiconductor Optoelectronic Devices Introduction to Physics and Simulation**, Elsevier Science (VSA), pp. (121-122), (2003).

88- K. S. Mobarhan, **"Test and Characterization of Laser Diode Determination of Principal Parameters"**, University California.

89- A. Joullie, P. Christol, A. N. Baranov and A. Vicet, **"Mid-infrared 2-5 µm Heterojunction Laser Diodes"**, Solid State Mid-infrared Laser Sources Topics Appl. Phys. Vol. 89, pp. (1-61), (2003).

90- H. K. Choi**, "Long-Wavelength Infrared Semiconductor Lasers", Published** in Canada, p. 35, (2004).

91- F. S. Mohammed and A. K. Hafiz, **"Strange Behavior in Semiconductor Laser Subjected to Optical Feedback at Different Temperature"**, Canadian Journal of Pure and Applied Science, Vol. 5, No. 2, pp. (1533-1540), (2011).

92- E. Farsad, S.P. Abbasi, A. Goodarzi and M. S. Zabihi, **"Experimental Parametric investigation of Temperature Effects on 60W-QCW Diode Laser",** World Academy of Science, Engineering and Technology, 59, pp. (1190-1195), (2011).

93- V. Panov and T. B. -Papancheva, **"Application of Ultraviolet light (UV) in dental Medicine"**, Literature Review, Medlnform, Iss. 2, pp. 194-200, (2015).

94- J. L. Pinedo V., F. Mireles G., C. Rios M., L. L. Quirino T. and J. I. Davila R., **"Spectral Signature of Ultraviolet Solar Irradiance in Zacatecas"**, Geofisica Internacional, Vol. 45, No. 4, pp. 263-269, (2006).

95- A. Asgari and S. Dashti, **"Optimization of Optical gain in $Al_xGa_{1-x}N/GaN/Al_xGa_{1-x}N$ Strained Quantum Well Laser"**, Optic 123, pp. (1546-1549), (2012).

96- P. M. Kowiak and W. O. Nakwaski, **"Threshold current of Nitride Vertical-Cavity Surface-Emitting Lasers with Various active regions"**, MRS Internet Journal Nitride Semiconductor Research 3, 35, pp. (1-10), (1998).

97- A. Baranov and E. Tournie, **Semiconductor Lasers: Fundamentals and Applications**, Woodhead Philadelphia New Delhi, p. 251, (2013).

98- M. Strassburg, J. Senawiratne, N. Dietz, U. Haboeck, A. Hoffmann, V. Noveski, R. Schlesser, and Z. Sitar, **"The Growth and Optical Properties of Large, High-Quality AlN Single Crystals"**, J. Appl. Phys., Vol. 96, No. 10, (2004).

الخلاصة

في هذا العمل تم تقديم دراسة نظرية لتحقيق أمثلية كثافة تيار العتبة لتركيب $Al_{0.01}Ga_{0.99}N/GaN$ الليزري المتعدد الآبار الكمية. وتتحقق هذه الدراسة من خلال تحديد افضل قيمة للعوامل المؤثرة على تيار العتبة و كثافة تيار العتبة لهذا التركيب كعدد الابار وعرض الحاجز من التركيز على افضل قيمة لعامل الحصر البصري. ثم حساب عرض البئر وانعكاسية مرآتي التجويف وطول التجويف وعرض التجويف ومعدل سمك المنطقة الفعالة وخسائر المرآة وكسب العتبة .

لقد وجد ان افضل قيمة لعامل الحصر البصري لليزر متعدد الابار الكمية عند عدد الابار ($N_w = 2$) وعرض الحاجز (b=2nm) عندما الطول الموجي (λ=352 nm) ضمن مدى الاشعة الفوق البنفسدية الطويلة (320-400 nm).

ان القيمة المثلى لكل من كثافة تيار العتبة (J_{th}=3743 A/cm^2) وتيار العتبة (I_{th}=14.97 mA) تم الحصول عليها عندما كان عرض البئر(w=4.3 nm) وانعكاسية المرآتين (R_1=0.75, R_2=0.9) وطول التجويف (L=2mm) وعرض التجويف (W=200 nm) ومعدل سمك المنطقة الفعالة (d=10.6 nm) وخسائر المرآة (α_m=0.98 cm^{-1}) وكسب العتبة (g_{th}=791cm^{-1}) عند درجة حرارة (T=300K).

تحقيق أمثلية كثافة تيار العتبة $Al_{0.01}Ga_{0.99}N/GaN$ لليزر متعدد الآبار الكمية

رسالة مقدمة الى

مجلس كلية التربية للعلوم الصرفة-ابن الهيثم ، جامعة بغداد

كجزء من متطلبات نيل درجة ماجستير علوم في الفيزياء

من قبل

كزال محمد قادر

بأشراف

د. ابتسام محمد تقي سلمان

1438ه   **2017م**